Contributions to Mineralogy and Petrology (2022) 177:51
https://doi.org/10.1007/s00410-022-01914-9

ORIGINAL PAPER

Mantle sources and melting processes beneath East Antarctica: geochemical and isotopic (Sr, Nd, Pb, O) characteristics of alkaline and tholeiite basalt from the Earth's southernmost (87° S) volcanoes

K. S. Panter[1] · Y. Li[1] · J. L. Smellie[2] · J. Blusztajn[3] · J. Reindel[1] · K. Odegaard[1] · M. J. Spicuzza[4] · S. Hart[3]

Received: 26 July 2021 / Accepted: 30 March 2022 / Published online: 17 April 2022

Abstract

Mount Early and Sheridan Bluff (87° S) are the above-ice expression of Earth's southernmost volcanic field and are isolated by > 1000 km from any other exposed Cenozoic volcano in Antarctica. These monogenetic, Early Miocene volcanoes consist of olivine-phyric basaltic pillow lavas and breccias (Mount Early) and pāhoehoe lavas (Sheridan Bluff) whose differentiation is controlled by the fractional crystallization of olivine with lesser quantities of clinopyroxene, plagioclase and magnetite. Fractional crystallization or contamination by crust cannot account for the coexistence of olivine tholeiite and alkaline compositions but their relationship can be explained by change from higher (5–6%) to lower (1.5–2%) degrees of partial melting concurrent with a decrease in peridotite−melt reaction in a mantle that is heterogeneous on a small-scale. Both magma types have geochemical and isotopic signatures that differentiate them from most of the volcanism found within the West Antarctic rift system. Data trends in Sr–Nd–Pb isotope space indicate mixing of at least two-distinct mantle sources: (1) a relatively depleted component similar to sources for mid-ocean ridge basalt from the extinct Antarctic–Phoenix spreading center, and (2) an enriched component similar to sources for mafic magmas of the Jurassic Karoo−Ferrar large igneous provinces. The availability of these mantle source types was facilitated by the detachment, sinking and heating of metasomatized continental lithosphere (enriched source) that released volatiles into the surrounding asthenosphere (depleted source) to promote flux melting. Volcanism triggered by lithospheric detachment is, therefore, explicitly applied to Mount Early and Sheridan Bluff to explain their isolation and enigmatic tectonic setting but also to account for source heterogeneity and the ephemeral change in degree of mantle partial melting recorded in their mafic compositions.

Keywords Olivine oxygen isotopes · Partial melting · Intraplate volcanism · Monogenetic volcanism · West Antarctic rift system · Lithospheric detachment

Introduction

Monogenetic basaltic volcanism is the most widespread type of magmatic activity on Earth and is typically expressed by fields of volcanic cones each of which formed by short-lived small-volume eruptions of a single, or only a few, batches of magma (Smith and Németh 2017). The low volume and restricted range of mafic compositions within most of these fields belie their complex origins. Detailed studies of individual centers and eruption sequences reveal that many are polymagmatic (i.e., several magma batches with distinct geochemical characteristics: e.g., Brenna et al. 2010; Van Otterloo et al. 2014). Most often, successive batches of mafic magmas shift from silica-undersaturated, incompatible trace element-enriched compositions (e.g., nephelinite, basanite, hawaiite) to more depleted silica-saturated/-oversaturated

Communicated by Othmar Müntener.

✉ K. S. Panter
kpanter@bgsu.edu

[1] School of Earth, Environment and Society, Bowling Green State University, Bowling Green, OH 43403, USA

[2] School of Geography, Geology and the Environment University of Leicester, Leicester LE1 7RH, UK

[3] Woods Hole Oceanographic Institution, Woods Hole, MA 02543, USA

[4] Department of Geoscience, University of Wisconsin-Madison, Madison, WI 53706, USA

compositions (e.g., alkali basalt, tholeiite) with time, though the opposite has been documented (e.g., Moore et al. 1995; Boyce et al. 2015). The shift in geochemistry can be explained by deep-seated processes that include changes in degree of mantle partial melting (e.g., Needham et al. 2011; Boyce et al., 2015) or variable inputs from mantle heterogenities (e.g., McGee et al., 2012; Gómez-Ulla et al. 2018) without chemical influence by crust. The comprehensive study of polymagmatic activity related to small-scale mafic systems can provide a real-time perspective on the conditions of their source regions and processes responsible for melt production and magma evolution. Here, we document the geochemical characteristics of monogenetic intraplate volcanism in East Antarctica. Our interpretations are based on data gathered from two basaltic volcanoes and yield important insights on the origin and nature of their sources and the cause of volcanism in a region that is relatively poorly understood.

The Mount Early and Sheridan Bluff volcanoes are situated approximately 300 km from the South Pole (c. 87° S, 153° W) and, therefore, are the two southernmost exposed volcanoes known on Earth. The volcanoes are found 15 km apart in the upper reaches of the Scott Glacier in the southern Transantarctic Mountains (Fig. 1). Mount Early and Sheridan Bluff are positioned on the margin of the East Antarctic craton, about 200 km inland from the Ross Sea boundary of the West Antarctic rift system (WARS) and,

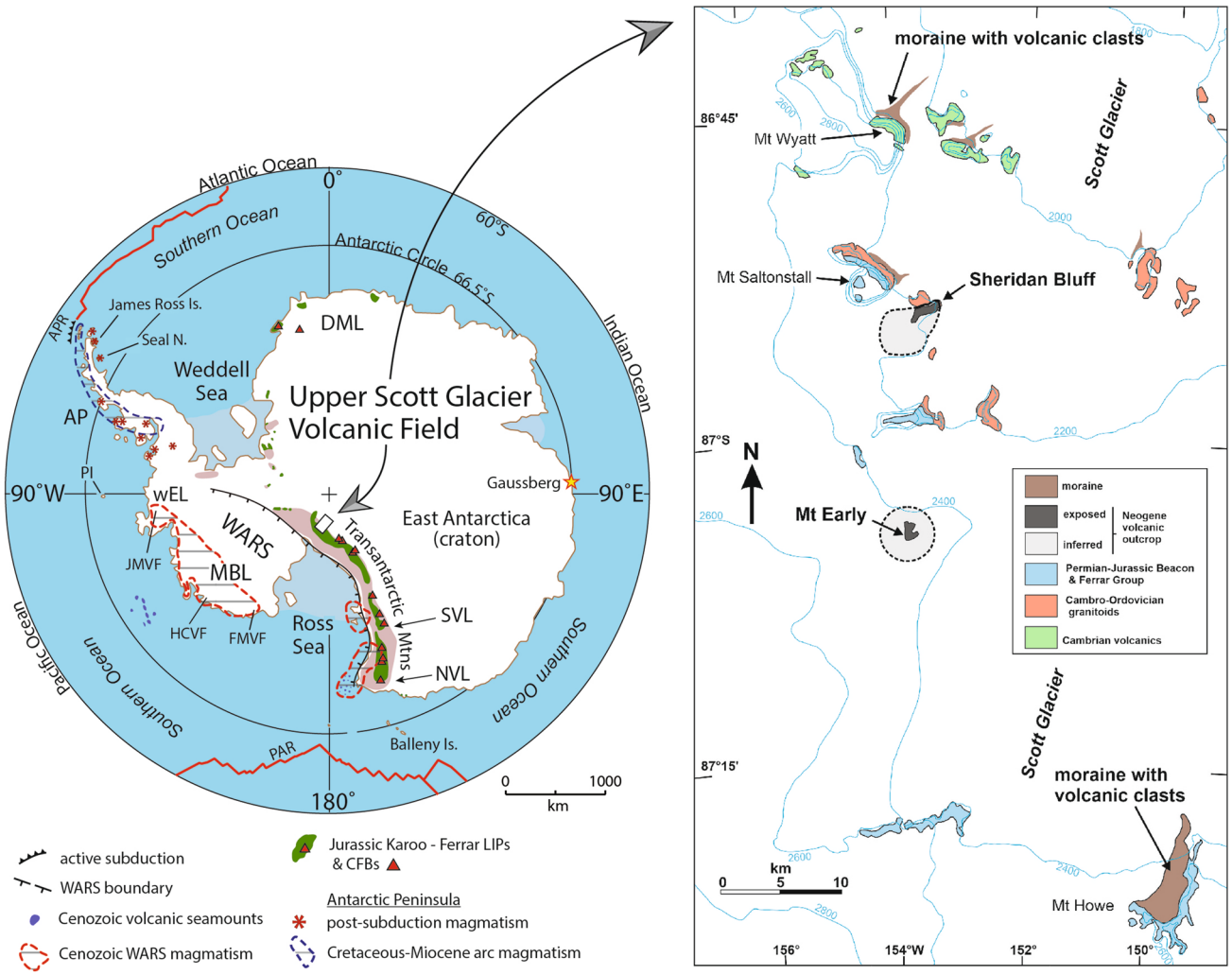

Fig. 1 Location maps. **A** Antarctica map showing the distribution of Mesozoic (Jurassic and Cretaceous) and Cenozoic magmatic provinces and volcanism. Distribution of Ferrar and Karoo large igneous provinces (LIPs) and associated continental flood basalts (CFBs) after Elliot and Fleming (2021) and Luttinen (2018). AP = Antarctic Peninsula, *APR* Antarctic−Phoenix Ridge, *DML* Dronning Maud Land, *FMVF* Fosdick Mountains Volcanic Field, *HCVF* Hobbs Coast Volcanic Field, *JMVF* Jones Mountains Volcanic Field, *MBL* Marie Byrd Land, *NVL* northern Victoria Land, *PAR* Pacific−Antarctic Ridge, *PI* Peter I Island, *SVL* southern Victoria Land, *wEL* western Ellsworth Land. **B** Geological map of the upper Scott Glacier, southern Transantarctic Mountains (modified from Smellie and Panter, 2021). The locations of Mount Early and Sheridan Bluff are shown, along with volcanic clasts found in several moraines beneath Mount Wyatt and Mount Howe, all of which make up the Upper Scott Glacier Volcanic Field—USGVF (Smellie et al., 2021b)

apart from a scattering of inland volcanoes in northern Victoria Land and the Gaussberg volcano located on the Wilhelm II Coast (Fig. 1), are the only exposed Cenozoic volcanoes in East Antarctica. This is in stark contrast to West Antarctica where Cenozoic volcanism is widespread and associated with the WARS as well as arc and post-arc volcanism on the Antarctic Peninsula (Fig. 1). Consequently, the occurrence, age and origin of volcanism in West Antarctica has been the focus of extensive investigations (e.g., LeMasurier and Thompson, 1990 and references therein; Smellie et al., 2021a and references therein). In this study our main focus is to understand the petrogenetic relationship between geochemically distinct batches of alkaline and subalkaline magmas to provide high-resolution information on mantle geochemical domains and melting conditions beneath the eastern portion of the continent. Although the Mount Early and Sheridan Bluff have been regarded as part of the WARS (i.e., included within the McMurdo Volcanic Group after Kyle 1990), they lie over 1000 km south of the major volcanic provinces found within the rift system (Fig. 1). In addition to being isolated geographically, we document that the mafic compositions from these volcanoes have geochemical and isotopic characteristics that are distinguishable from the majority of WARS volcanism, suggesting contributions from different sources. Furthermore, the trigger for melting beneath this region is also atypical of mechanisms that have been proposed for melting beneath the WARS and may be applicable to other monogenetic intraplate volcanism in Antarctica and elsewhere.

This study of Mount Early and Sheridan Bluff volcanoes was initiated by fieldwork in 2015 that is described by Smellie et al. (2021b) and is an extension of a preliminary geochemical investigation of the basalts by Panter et al. (2021a). Here, we present radiogenic isotopes (Sr, Nd and Pb) of whole rock samples and oxygen isotopes from olivine as well as trace elements measured on six additional samples. The previous petrological findings, which are based solely on major and trace element abundances, suggested that some magmas may have assimilated continental crust. Thus, a major goal for obtaining isotopic data was to examine this hypothesis and to further evaluate compositional characteristics that may distinguish between discrete mantle sources. Below we argue that mantle domains identified in this study are akin to sources that have been sampled by mafic volcanism on the Antarctic Peninsula (Miocene-Recent back-arc and post-subduction intraplate basalts) and two widely separated mafic volcanic fields in West Antarctica (the Jones Mountains and basaltic centers found within the Fosdick Mountains, Fig. 1). Furthermore, we explore whether melt compositions were influenced by mantle sources associated with widespread Jurassic magmatism that produced the Karoo–Ferrar large igneous provinces (Fig. 1).

Volcanological and petrological background

Mount Early and Sheridan Bluff are two Early Miocene monogenetic volcanoes exposed above the East Antarctic Ice Sheet at the head of the Scott Glacier (Fig. 1). Mount Early (2850 m above sea level, masl) forms a well exposed conical nunatak while Sheridan Bluff (2570 masl) is a less prominent and highly dissected small-volume shield volcano. The volcanoes are part of the newly designated Upper Scott Glacier Volcanic Field (USGVF, Smellie et al. 2021b) which constitutes a much larger area of Miocene volcanism inferred to lie beneath the East Antarctic Ice Sheet. The extent of the Upper Scott Glacier Volcanic Field is based on the discovery of clasts of alkaline basalt recovered from moraines at Mount Howe (Licht et al. 2018), which is c. 30 km south (up-stream) of Mount Early, and from Mount Wyatt (E. Stump, personal communication, 2014) that lies c. 15 km north of Sheridan Bluff. The Early Miocene age of the USGVF is constrained based on radiometric dating and ranges from 15.45 to 20.6 Ma (Stump et al. 1980; Licht et al. 2018). Smellie et al. (2021b) and Smellie and Panter (2021) provided a detailed account of the volcanology and stratigraphy of Mount Early and Sheridan Bluff that includes reconstruction of paleo-environmental conditions during eruption and constraints on the thickness of the East Antarctic Ice Sheet in the Early Miocene. Mount Early consists of a large mound of pillow lavas overlain by a thin drape of lapilli tuff with an exposed thickness of at least 450 m, together with irregular intrusions and rare dykes. It is interpreted to have been subglacially erupted, probably beneath an ice stream (Stump et al. 1980; Smellie et al. 2021b; Smellie and Panter 2021). Deposits at Sheridan Bluff lie on top of a glacially striated granitoid surface and include lava flows that show an overall flow pattern that radiates away from what was likely a central cone composed of lapilli tuff. The main cliff exposure at Sheridan Bluff consists of lapilli tuff conformably overlain by a c. 110-m-thick succession of pāhoehoe lavas separated by red scoriaceous surfaces. Smellie et al. (2021b) interpreted Sheridan Bluff volcano to be a small basaltic shield volcano. Despite the evidence for glacial conditions both prior to and post-dating eruption, the Sheridan Bluff edifice was probably erupted in an ice-poor or conceivably ice-free setting (Smellie and Panter 2021).

Panter et al. (2021a) presented a detailed account of the major and trace element characteristics and the petrogenesis of basaltic compositions at Mount Early and Sheridan Bluff. The data set also includes samples and analyses provided by Stump et al. (1980; 1990a, b) and Licht et al. (2018). Overall, the basalts show a relatively broad range in MgO content (4–10 wt.%) with a very narrow range in SiO_2 content (49–51 wt.%) and are classified as olivine tholeiite, hawaiite and mugearite (Fig. 2). Olivine tholeiite lavas are subalkaline (up to 6 wt.% hypersthene-normative) and are

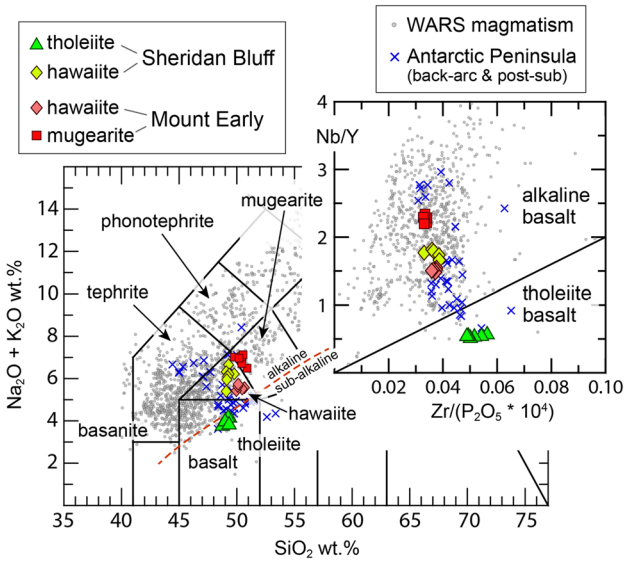

Fig. 2 Classification of Mount Early and Sheridan Bluff compositions on a total alkali versus silica diagram (after Le Bas et al., 1986) and a discriminant plot between alkaline and tholeiite basalt (inset) from Floyd and Winchester (1975). All major and trace elements for samples from Mount Early and Sheridan Bluff are given in Table S1. Other data shown are Cenozoic igneous rocks from all provinces within the West Antarctic rift system complied by Panter et al. (2021b), Martin et al. (2021) and Rocchi and Smellie (2021) and Miocene−Recent back-arc and post-subduction intraplate basalts (several samples classify as tholeiite—*see inset*) from the Antarctic Peninsula (data sources: Hole 1988; Hole et al. 1993a; Kosler et al. 2009; Hole 2021). All samples are normalized to 100% volatile free and those plotted on the basalt discriminant diagram (inset) are limited to samples with SiO_2 contents that range from 40 to 51 wt.%. The dashed line delimiting alkaline from subalkaline compositions on the TAS plot is from Irvine and Baragar (1971)

exclusively found in the main cliff section at Sheridan Bluff where they are conformably overlain by hawaiite lavas that range from mildly subalkaline (< 1.1 wt.% hypersthene-normative) to mildly alkaline (< 1.6 wt.% nepheline-normative) compositions. All hawaiite and mugearite samples from Mount Early are alkaline (2–6 wt.% nepheline-normative). Olivine tholeiite has the lowest concentrations of TiO_2 and P_2O_5 relative to all other samples in the suite as well as the lowest incompatible trace element concentrations [e.g., light rare earth elements (LREE), Ba, Nb, Ta, Sr and Zr]. Mount Early and Sheridan Bluff samples show an overall decrease in concentrations of FeO^T, CaO and compatible trace elements (e.g., Cr, Sc and Ni) and an increase in all other major and incompatible trace elements with decreasing MgO content. These trends are broadly consistent with magmatic evolution by fractional crystallization dominated by the removal of olivine and clinopyroxene. Panter et al. (2021a) quantitatively evaluated the process of fractional crystallization using several models (i.e., least-squares mixing combined with Rayleigh distillation and solutions using the MELTS algorithm from Ghiorso and Sack (1995) that were constrained by petrographic observations, mineral chemistry and thermobarometric estimates. The models were unsuccessful in relating the basalts to a single liquid line of descent and demonstrated that the alkaline compositions cannot be derived from a tholeiitic magma by fractional crystallization. Samples with high Cs contents, low Ce/Pb ratios and that lack negative K and Pb concentration spikes on mantle normalized multi-element diagrams may be the result of contamination by crust during magma ascent to the surface. However, simple mixing and assimilation−fractional crystallization (AFC) models for the contamination of olivine tholeiite by upper continental crust failed to produce the compositions of coexisting hawaiite lavas found at Sheridan Bluff (Panter et al. 2021a).

The intimacy in time and space of the olivine tholeiite and hawaiite lavas erupted at Sheridan Bluff is considered to be a consequence of different degrees of partial melting of a common mantle source (Panter et al. 2021a). This assertion is based on the fact that both compositional types have similar concentrations in Y and heavy REEs (HREE) but progressively diverge for elements with increasing incompatibility as illustrated on multi-element normalized plots. Melting proportions were also modeled using non-modal batch melting of amphibole-bearing garnet lherzolite and indicate higher degrees of melting to generate magmas parental to tholeiites relative to those for alkaline compositions. Scenarios involving near-simultaneous melting at different depths or rapid decrease in melt proportion resulting from exhaustion of more easily fusible phases were suggested by Panter et al. (2021a) to explain the contemporaneous eruption of these two magma types. The detachment and dehydration of metasomatized mantle lithosphere likely facilitated the melting beneath this region (Shen et al. 2018; Licht et al. 2018; Panter et al. 2021a).

Panter et al. (2021a) also compared Mount Early and Sheridan Bluff samples with WARS compositions, specifically basalts from the McMurdo Volcanic Group in the western Ross Sea (Fig. 1) and pointed out several key differences with respect to major and trace element concentrations. A similar comparison is made here in Fig. 3 but with a more comprehensive suite of WARS samples that include basaltic compositions from the Marie Byrd Land Volcanic Group (Panter et al. 2021b) in addition to low-Ti basalts (≤ 1 wt.% TiO_2) from the Karoo−Ferrar large igneous provinces (LIPs) and Miocene-Recent back-arc and post-subduction intraplate basalts from the Antarctic Peninsula. Mount Early and Sheridan Bluff samples plot away from most WARS basalts, having lower FeO^T and TiO_2 contents and higher Al_2O_3/TiO_2 ratios over an equivalent range of MgO wt.% (Fig. 3). Note, however, that Mount Early and Sheridan Bluff compositions closely

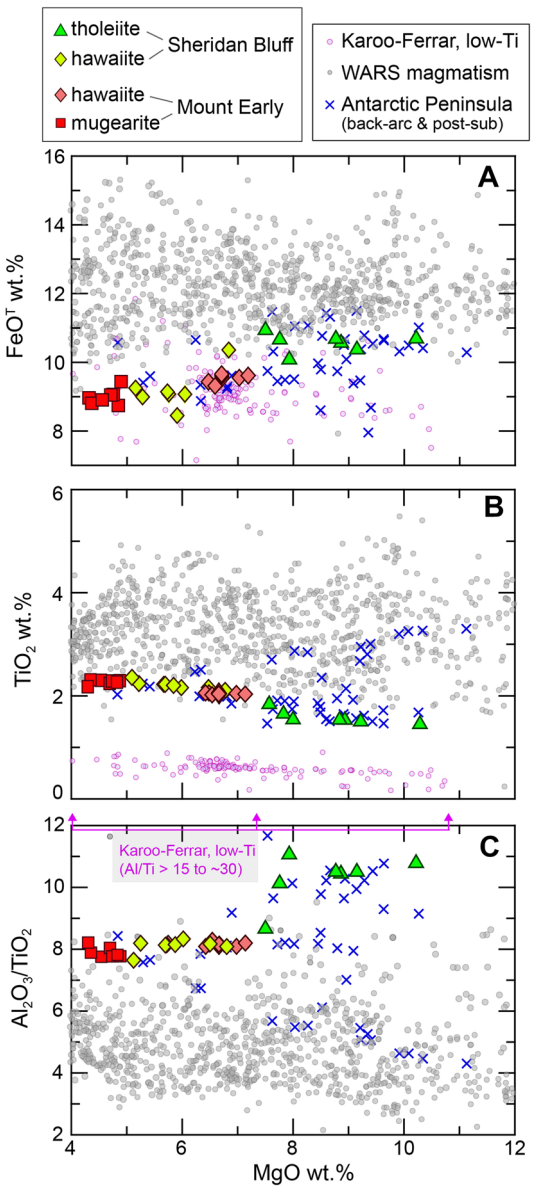

Fig. 3 Variations in whole rock MgO wt.% versus FeO^T (**A**), TiO_2 (**B**) wt % and Al_2O_3/TiO_2 ratios (**C**). Karoo−Ferrar low-Ti ($\leq$1 wt.% TiO_2) basalts (SiO_2 40–55 wt.%) are from the GEOROC data base (http://georoc.mpch-mainz.gwdg.de/georoc/) and in (**C**) plot off-scale at higher Al/Ti ratios (> 15 to ~ 30) over the range of MgO from 4 to 10.7 wt.%. Other symbols and data sources are the same as in Fig. 2

match many alkaline basalts (and rare tholeiite) from the Antarctic Peninsula and have similar FeO^T contents relative to many of the low-Ti samples from the Karoo−Ferrar LIPs. The TiO_2 concentrations for Sheridan Bluff and Mount Early samples are higher than Karoo−Ferrar compositions but notably show sub-parallel trends (Fig. 3). We discuss in detail below, with the addition of isotopic data, that these relationships provide evidence of sources that are fundamentally different from sources for most WARS volcanism.

Sample details and analytical methods

A total of 31 basaltic samples were collected from Mount Early and Sheridan Bluff for petrological investigations. Eight additional samples were collected and analyzed by Stump et al. (1980; 1990a, b) for major and minor elements and six of those were measured for trace elements and isotopes of Sr, Nd and Pb for this study. Field observations, petrographic characteristics, mineral chemistry and whole rock major and trace element concentrations for the other 23 samples collected in 2015 are provided by Reindel (2018) and Panter et al. (2021a). In this study, we present whole rock isotope analyses for Sr, Nd and Pb ($n = 13$ samples) as well as mineral chemistry and oxygen isotopes for olivine ($n = 22$ samples) that were first reported by Li (2020). A complete set of geochemical analyses is provided in Table S1 and isotope analyses are provided in Tables 1 and 2.

Olivine chemistry

Olivine mineral chemistry was measured at the Electron Microbeam Analysis Laboratory (EMAL), University of Michigan, using a Cameca SX-100 set at 20 kV accelerating voltage beam, 40 nA beam current and 2 µm spot size. The peak counting times range from 10 to 30 s. Olivine phenocrysts in 22 samples were analyzed. Reindel (2018) measured 3 to 4 olivine phenocrysts within each of eight samples and Li (2020) measured 10 to 12 grains within each of the remaining fourteen samples. Over 480 spot analyses of olivine phenocrysts are presented in supplementary Table S2. The majority of analyses are from the middle of grains (*cores*) but spot analyses within c. 20 µm of grain edges (*rims*) were also taken to evaluate compositional zoning. The weight percentage concentrations of six major and minor element oxides (SiO_2, FeO^T, NiO, MnO, MgO, and CaO) were measured on all olivine phenocrysts. In addition, Al_2O_3, Cr_2O_3, and TiO_2 wt.% contents were measured for olivine in 8 samples by Reindel (2018). Analytical error based on counting statistics average < 0.5% for major element oxides with concentrations of greater than 10 wt.% and for minor element oxides with concentrations less than 1 wt.% the average error is < 6.5%. Cations are calculated based on four oxygens in the idealized formula and the forsterite content (Fo%) equals 100*[Mg/(Mg + Fe)]. Although Fo% varies between samples (see Results), the spot values near grain edges (*rims*) are consistently lower than near *core* values. The *rims* of grains are mostly thin (c. < 5 µm based on backscatter electron images—BSE, Fig. 4) and are assumed to comprise no more than about 1% of the total volume of a

Table 1 Sample summary and olivine data for Mount Early and Sheridan Bluff, Upper Scott Glacier Volcanic Field, Antarctica

Sample	Rock type	Sample/lithofacies and sequence [1]	MgO_{WR} wt.%	Fo% [2]	Run 1 $\delta^{18}O$ ‰ [3]	Run 2 $\delta^{18}O$ ‰ [3]	Δ	Avg $\delta^{18}O$ ‰	T (°C) [4]	Equil melt [5] $\delta^{18}O$ ‰
Mount Early										
ME15-001	Hawaiite	Lava pillow interior	7.01	83.0	5.48	5.55	− 0.07	5.52	–	*6.32*
ME15-003	Mugearite	Dike interior	4.86	74.2	5.61	5.58	0.03	5.60	1202	6.41
ME15-004	Hawaiite	Lava pillow interior	6.65	82.9	5.53	5.52	0.01	5.53	1241	6.30
ME15-005b	Hawaiite	Columnar jointed dike	6.50	80.6	5.46	5.54	− 0.08	5.50	1237	6.28
ME15-006	Hawaiite	Lava block in lapilli tuff	6.59	79.6	5.57	5.47	0.1	5.52	1235	6.30
ME15-007	Hawaiite	Lava block in lapilli tuff	6.40	80.8	5.40	–	–	5.40	1230	6.18
ME15-008	Hawaiite	Lava pillow interior	6.46	80.9	5.49	5.30	0.19	5.40	1230	6.18
ME15-009	Mugearite	Dike interior	4.71	75.5	5.70	5.67	0.03	5.69	1181	6.52
ME15-010	Mugearite	Dike interior	4.20	75.0	5.73	5.72	0.01	5.73	1117	6.64
ME15-011	Mugearite	Scoria in lapilli tuff	4.27	75.6	5.09	5.50	− 0.41	5.30	1135	6.19
ME15-012	Mugearite	Dike interior	4.64	76.2	5.51	5.64	− 0.13	5.58	1148	6.45
ME15-013	Mugearite	Lava clast in breccia	4.41	75.7	5.27	5.19	0.08	5.23	1118	6.15
ME15-014	Hawaiite	Lava pillow interior	6.95	83.3	5.42	5.55	− 0.13	5.49	–	*6.29*
Sheridan Bluff										
SB15-001	Tholeiite	Lava flow interior (1-base)	10.19	83.7	5.49	5.01	0.48	5.25	1328	5.93
SB15-002	Tholeiite	Lava flow interior (1-base)	8.78	83.4	5.57	5.57	0.00	5.57	1266	6.30
SB15-003	Hawaiite	Lava flow interior (5-'top')	5.09	80.4	5.78	5.87	− 0.09	5.83	–	*6.63*
SB15-004	Tholeiite	Lava flow interior (2-lower)	7.49	80.4	5.49	5.55	− 0.06	5.52	1249	6.27
SB15-005	Tholeiite	Lava flow interior (3-middle)	7.86	–	–	–	–	–	–	–
SB15-006	Hawaiite	Lava flow interior (4-upper)	6.49	81.6	–	5.57	–	5.57	–	*6.37*
SB15-007	Hawaiite	Lava (float)	5.21	79.7	5.71	5.95	− 0.24	5.83	–	*6.63*
SB15-008	Hawaiite	Lava flow interior	6.01	81.3	5.67	5.71	− 0.04	5.69	–	*6.49*
SB15-009	Tholeiite	Lava flow interior	8.72	83.2	5.55	5.74	− 0.19	5.65	1279	6.37
SB15-010	Hawaiite	Lava flow interior	5.69	81.3	5.81	5.67	0.14	5.74	1194	6.56

[1]Sequence = order of stratigraphic sequence for 5 lava flows exposed in the main cliff section at Sheridan Bluff

[2]Forsterite content of olivine [Fo% = (Mg/Mg + Fe)*100] is calculated as a weighted average based on the volume proportion of *core* to *rim* equal to 99:1 (refer to Table S2)

[3]Corrected $^{18}O/^{16}O$ ratios are reported in $\delta^{18}O$ notation relative to Vienna standard mean ocean water, VSMOW

[4]Temperatures based on olivine chemistry (Table S5) using the averaged solutions of Eqs. 21 and 22 from Putirka (2008)

[5]Oxygen isotope composition of melt in equilibrium with olivine calculated using: $10^3 \ln \alpha_{olivine-basalt} = A \times 10^6/T^2$; where A = − 1.74 for tholeiite and − 1.77 ('basalt') for the rest of the samples (values from Zhao and Zheng, 2003). *T* is in Kelvin. Oxygen isotope melt values shown in italics are calculated using an average olivine-melt fractionation of 0.80

grain. Therefore, the Fo% is calculated as a weighted average based on the volume proportion of *core* to *rim* equal to 99:1. All spot analyses in the proportion 99:1 (*core:rim*) are used to calculate the composition of individual olivine grains (Table S2) and the overall average composition of olivine for each sample (Table 1).

Olivine oxygen isotopes

Oxygen isotopes were measured on olivine phenocrysts at the University of Wisconsin-Madison, Department of Geoscience, Stable Isotope Laboratory using laser fluorination–gas source mass spectrometry. Twenty-two olivine-phyric samples were crushed and sieved to obtain 425–850 µm grain-size fractions. Olivine was then hand-picked and only the best grains (i.e., euhedral and clear with minimal or no inclusions) were selected. Olivine separates were cleaned with deionized water in an ultrasonic bath to remove any adhering matrix. Two milligram aliquots (c. 4–5 grains) of olivine were loaded with a standard into separate holes in a Ni-sample holder and pumped to vacuum before adding a small amount of BrF_5 reagent as a pre-treatment. Samples and standard were individually heated using a CO_2 laser fluorination system attached to a dual-inlet five-collector Finnigan MAT 251 mass spectrometer. Corrected $^{18}O/^{16}O$ ratios are reported in $\delta^{18}O$ notation (per mil variations relative to Vienna standard mean ocean water, VSMOW) and calibrated against the UWG-2 Gore Mountain garnet standard ($\delta^{18}O_{VSMOW} = 5.80‰$, Valley et al. 1995). The average $\delta^{18}O$ value of UWG-2 standard measured over a two-day

Table 2 Sr–Nd–Pb isotope ratios for Mount Early and Sheridan Bluff samples

Sample	Rock type	$^{87}Sr/^{86}Sr$	$^{143}Nd/^{144}Nd$	$^{206}Pb/^{204}Pb$	$^{207}Pb/^{204}Pb$	$^{208}Pb/^{204}Pb$
Mount Early						
ME15-003	Mugearite	0.704386	0.512858	18.816	15.622	38.542
ME15-004	Hawaiite	0.704750	0.512771	18.816	15.629	38.561
ME15-005b	Hawaiite	0.704767	0.512824	18.824	15.632	38.572
ME15-009	Mugearite	0.704506	0.512816	18.807	15.623	38.534
ME15-011	Mugearite	0.704446	0.512818	18.826	15.626	38.563
ME15-014	Hawaiite	0.704680	0.512831	18.821	15.630	38.567
ANT32	Hawaiite	0.704857	0.512761	18.829	15.644	38.599
ANT34	Mugearite	0.704640	0.512759	18.794	15.617	38.692
Sheridan Bluff						
SB15-001	Tholeiite	0.704851	0.512775	18.767	15.637	38.533
SB15-004	Tholeiite	0.704803	0.512756	18.677	15.626	38.416
SB15-005	Tholeiite	0.704324	0.512812	18.827	15.629	38.540
SB15-006	Hawaiite	0.703832	0.512901	18.906	15.614	38.592
SB15-008	Hawaiite	0.703899	0.512869	18.888	15.628	38.660
SB15-009	Tholeiite	0.704867	0.512731	18.776	15.635	38.531
SB15-010	Hawaiite	0.703848	0.512860	18.882	15.614	38.614
ANT21	Tholeiite	0.704850	0.512735	18.788	15.617	38.417
ANT23	Tholeiite	0.704387	0.512793	18.809	15.618	38.479
ANT25	Hawaiite	0.703899	0.512848	18.911	15.614	38.588
ANT29	Hawaiite	0.703952	0.512844	18.873	15.612	38.566

Sr, Nd and Pb isotopes were measured by MC-ICP-MS ("ME" and "SB") and by TIMS ("ANT")

Sr data are corrected against SRM987 standard $^{87}Sr/^{86}Sr = 0.710240$

Nd results are corrected against JNdi-1 standard $^{143}Nd/^{144}Nd = 0.512104$

Pb analysis are corrected against NBS981 standard (Todt et al., 1996)

period ($n = 16$) was 5.79 ± 0.08‰ (2 sigma standard error, 2SSE). Two analyses of olivine grains from each rock were performed and most have differences in $\delta^{18}O$ values between aliquots (run 1 and 2) that are ≤ 0.19 ‰ (Table 1). However, replicate aliquots for three samples, ME15-011, SB15-001 and SB15-007, have much larger differences ($\Delta = 0.41$‰, 0.48‰, and 0.24‰, respectively) and these samples also have the lowest and highest $\delta^{18}O$ values (5.01‰, 5.09‰ and 5.95‰, respectively) of the 22 samples measured (Table 1). Sample heterogeneity is credited for these variations and is supported by the greater number of melt inclusions and opaque oxides (magnetite?) observed within olivine phenocrysts separated from these basalts.

Radiogenic isotopes (Sr, Nd, and Pb)

Isotopes of Sr, Nd and Pb were measured on a NEPTUNE multi-collector ICP-MS at the Woods Hole Oceanographic Institution (WHOI) for samples collected in 2015 with prefix "ME" and "SB" (Table 2). Whole rock powders for 13 samples were dissolved in 3:1 mixture of concentrated HF:HNO_3, followed by three dry-downs in 6.2 N HCl to convert fluorides to chlorides. Separation of Sr and Nd was carried out with Eichrom Sr-Spec and Ln-Spec resin, respectively. Lead was separated following the HBr–HNO_3 procedure of Abouchami et al. (1999) using a single column pass. For Sr and Nd, the internal precision is 10–20 ppm (2σ); external precision, after adjusting to 0.710240 and 0.512104 for the SRM987 Sr and JNdi-1 Nd standards respectively, is estimated to be 15–25 ppm (2σ). Lead analyses carry internal precisions on 206, 207, 208/204 ratios of 15–50 ppm; SRM997 Tl was used as an internal standard, and external reproducibility (including full chemistry) ranges from 17 ppm (2σ) for $^{207}Pb/^{206}Pb$, to 120 ppm (2σ) for $^{208}Pb/^{204}Pb$. The Pb isotope ratios were corrected to the reported values for the NBS981 standard (Todt et al. 1996). Samples with prefix "ANT" (Table 2) were collected by Ed Stump et al. in 1978–1979 and were analyzed by thermal ionization mass spectrometry (TIMS) using a VG-354 multi-collector instrument at the WHOI and the analytical details follow those that are described by Saal et al. (2007). Sr and Nd isotope data carry 2σ precisions of ± 35 ppm and ± 40 ppm and are reported relative to 0.71024 (SRM 987 standard) and 0.512104 (JNdi-1 standard), respectively. Pb isotopic results are corrected against NBS981, values from Todt et al. (1996). Reproducibility of the Pb runs is 0.02% per amu based on repeat runs of NBS981.

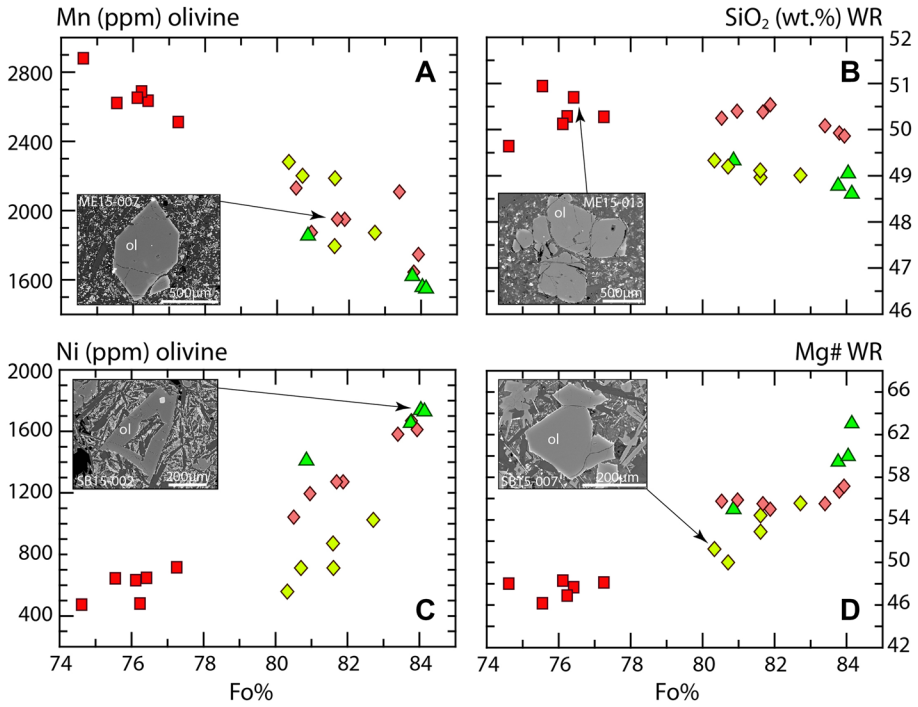

Fig. 4 Forsterite content (Fo%) of olivine phenocrysts from Mount Early and Sheridan Bluff plotted against olivine trace elements Mn (**A**) and Ni (**C**) in parts per million (ppm) as well as whole rock (WR) SiO_2 concentrations (**B**) and whole rock magnesium number [Mg# = 100*(Mg/(Mg + Fe^{2+})]. Each sample's olivine composition is a weighted average of all spot analyses (Tables 1 and S2). In addition, shown are representative back-scatter electron (BSE) images of phenocrystic and glomerocrystic olivine in selected samples. The skeletal olivine in sample SB15-002 (**c**) is interpreted, along with coexisting swallow-tailed plagioclase grains, to be textures produced by rapid undercooling (i.e., quenching). Symbols for Sheridan Bluff and Mount Early samples are the same as in Fig. 2

Results

Olivine textures and composition

Forsteritic olivine (Fo% 75−84; Table 1) and plagioclase (An% 48−67) are the most abundant phenocrysts (3 to 15% by volume) in basaltic compositions at Sheridan Bluff and Mount Early along with lesser amounts of clinopyroxene (diopside and augite, Wo% > 43) and microphenocrysts of titaniferous magnetite, ilmenite and Cr-spinel (Reindel 2018; Panter et al. 2021a). Overall, the phenocrysts appear to have been in equilibrium with coexisting liquid although reaction and resorbed textures are observed in a few large plagioclase grains (antecrysts?). Olivine phenocrysts range from euhedral to subhedral and mostly display homogeneous grey tones on BSE images with very thin bright *rims* (Fig. 4). The spot analyses near the *rims* have lower Fo% relative to spot analyses taken near the *cores* of the grains. Weighted average forsterite contents show a systematic decrease with increasing olivine Mn concentration and whole rock SiO_2 wt.% (Fig. 4a,b) and with decreasing olivine Ni concentration and whole rock Mg# = 100*[Mg/(Mg + Fe)] (Fig. 4c,d). The trends suggest that variations in olivine composition are most likely controlled by the fractional crystallization process.

Olivine $\delta^{18}O$ values

The total range of $\delta^{18}O$ measured on olivine ($n_a = 42$, c. 4–5 grains per analysis) is 5.01–5.95 ‰ (Table 1) with an overall mean value of 5.54 ± 0.06‰ (all errors are reported as 2σ standard error of mean, 2SSE). The range in $\delta^{18}O$ for the 22 samples based on averaged values of both aliquots is not significantly different at 5.23 to 5.83‰ with a mean of 5.55‰ ± 0.07‰. Excluding the three samples that show large differences between aliquots (ME15-011, SB15-001 and SB15-007, Table 1) the mean of the remaining 19 samples (5.56 ± 0.06 ‰) is indistinguishable from the overall mean and the 22-sample mean. Furthermore, there is no significant difference in $\delta^{18}O$ values between Mount Early and Sheridan Bluff (5.50 ± 0.08 ‰ and 5.63 ± 0.12 ‰, respectively).

The relatively uniform oxygen isotopic values for olivine from basalts at Mount Early and Sheridan Bluff are significantly higher than average upper mantle olivine ($\delta^{18}O = 5.18 \pm 0.03$ ‰, $n_a = 76$, Mattey et al. 1994) and average olivine in WARS basalts ($\delta^{18}O = 5.17 \pm 0.09$‰,

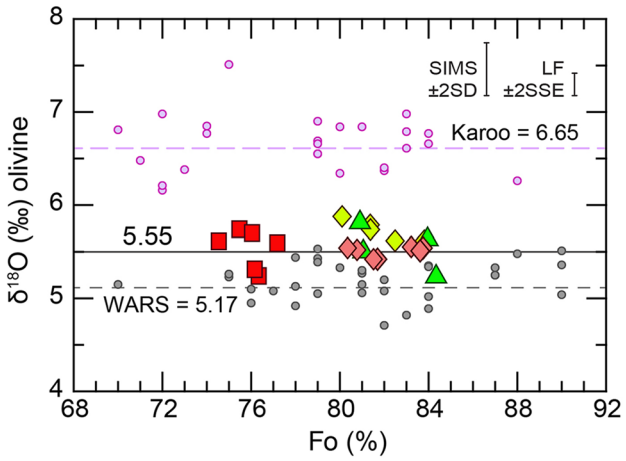

Fig. 5 Olivine Fo% plotted against $\delta^{18}O_{olivine}$ for Sheridan Bluff and Mount Early samples and compared to olivine in basalts from the WARS (Mortimer et al. 2007; Nardini et al. 2009; Panter et al. 2018) and from continental flood basalts (CFB) of the Karoo large igneous province in Antarctica (Heinonen et al., 2018). An average error bar at 2 sigma standard error (2SSE) is representative of $\delta^{18}O$ olivine analyses measured by laser fluorination (this study, Table 1) as well as for WARS samples measured by laser fluorination (see Panter et al., 2018). Olivine collected from Karoo lavas (Antarctica) and the majority of WARS samples from the NW Ross Sea were measured by secondary ionization mass spectrometry (SIMS). An average error at two times the standard deviation (2SD) for SIMS analyses based on San Carlos olivine is also shown. Overall averaged $\delta^{18}O$ of olivine for each sample suite are marked by horizontal solid and dashed lines; Sheridan Bluff and Mount Early = 5.55‰, WARS = 5.17‰, Karoo CFB = 6.65‰

$n_a = 37$) from the northwestern Ross Sea measured by both laser fluorination and SIMS techniques (Fig. 5) and even higher if only analyses by laser fluorination ($\delta^{18}O = 5.03 \pm 0.11$‰, $n_a = 9$) are considered (Panter et al. 2018). As shown in Fig. 5, Mount Early and Sheridan Bluff samples are also significantly lower than olivine in Jurassic continental flood basalts from the Karoo large igneous province (LIP), Dronning Maud Land ($\delta^{18}O = 6.2-7.5$‰, Heinonen et al. 2018). Rocks from the Ferrar LIP, broadly associated with the Karoo magmatic event, are exposed within the Transantarctic Mountains and are found within the vicinity of Mount Early and Sheridan Bluff. Whole rock $\delta^{18}O$ values for lavas from the Ferrar (i.e., Kirkpatrick Basalt) average c. 7.0‰ (Hoefs et al. 1980; Kyle et al. 1983; Mensing et al. 1984; Molzahn et al. 1996). This value is close to the average value of 7.4 ‰ calculated for melt in equilibrium with olivine in Karoo lavas (Heinonen et al. 2018). The origin of elevated oxygen isotopic signatures (along with high Sr and low Nd isotopic ratios) in Ferrar−Karoo flood basalts has been a subject of debate as to whether they are the result of crustal contamination (e.g., by AFC) or contribution from isotopically enriched mantle sources (see Elliot and Fleming, 2021 and references therein).

Isotopes of Sr, Nd and Pb

Radiogenic isotope ratios for Mount Early and Sheridan Bluff samples are reported in Table 2 and shown in Fig. 6 along with Cenozoic basaltic compositions from the WARS and Miocene-Recent alkaline basalts from the Antarctic Peninsula. In addition, shown are compositions from the Jurassic Ferrar−Karoo LIPs in Antarctica but it is important to note that most these samples plot off-scale in Fig. 6A and B, trending towards higher Sr and lower Nd isotope ratios. In addition, note that a few samples of Ferrar–Karoo plot off-scale in Fig. 6C and D; however, the majority of data points lie within the plot. Sheridan Bluff and Mount Early are more radiogenic with regards to their Sr isotopes (0.703832−0.704867) and their Nd isotopic ratios extend to less radiogenic values (0.512731−0.512901) compared to nearly all WARS and Antarctic Peninsula back-arc and intraplate basalts (Fig. 6). Lead isotopic ratios are relatively un-radiogenic (18.677−18.906, 15.614−15.637 and 38.416−38.660 for $^{206}Pb/^{204}Pb$, $^{207}Pb/^{204}Pb$ and $^{208}Pb/^{204}Pb$, respectively) and partially overlap with some mid-ocean ridge basalts (MORB) from the active Pacific–Antarctic Ridge and the extinct Antarctic–Phoenix Ridge (Fig. 1; PAR and APR, respectively, in Fig. 6C and D). In addition, they have lower Pb values than most WARS samples but are similar to most Antarctic Peninsula intraplate basalts and those from the Fosdick Mountains in western Marie Byrd Land and the Jones Mountains from western Ellsworth Land (Fig. 1). Endmember compositions for the Sheridan and Early suite are defined by hawaiite sample SB15-006, having the lowest $^{87}Sr/^{86}Sr$ and $^{207}Pb/^{204}Pb$ ratios and highest $^{143}Nd/^{144}Nd$ and $^{206}Pb/^{204}Pb$ ratios, and olivine tholeiite samples SB15-001, -004 and -009 have the most enriched Sr and Nd isotopic signatures (Table 2). These samples were collected within a conformable c. 110-m-thick succession of lava flows exposed in the main cliff section at Sheridan Bluff.

Discussion

A key objective for this study is to critically evaluate prior interpretations on magma origin and evolution at Mount Early and Sheridan Bluff (Panter et al. 2021a) with the addition of analyses for Sr, Nd, Pb and O isotopes. More specifically, we attempt to decipher whether some compositional characteristics reflect assimilation of crust or the melting of an enriched source(s) and to determine the petrogenetic relationship between tholeiite and alkaline magmas. Solving these conundrums are common goals for studies focused

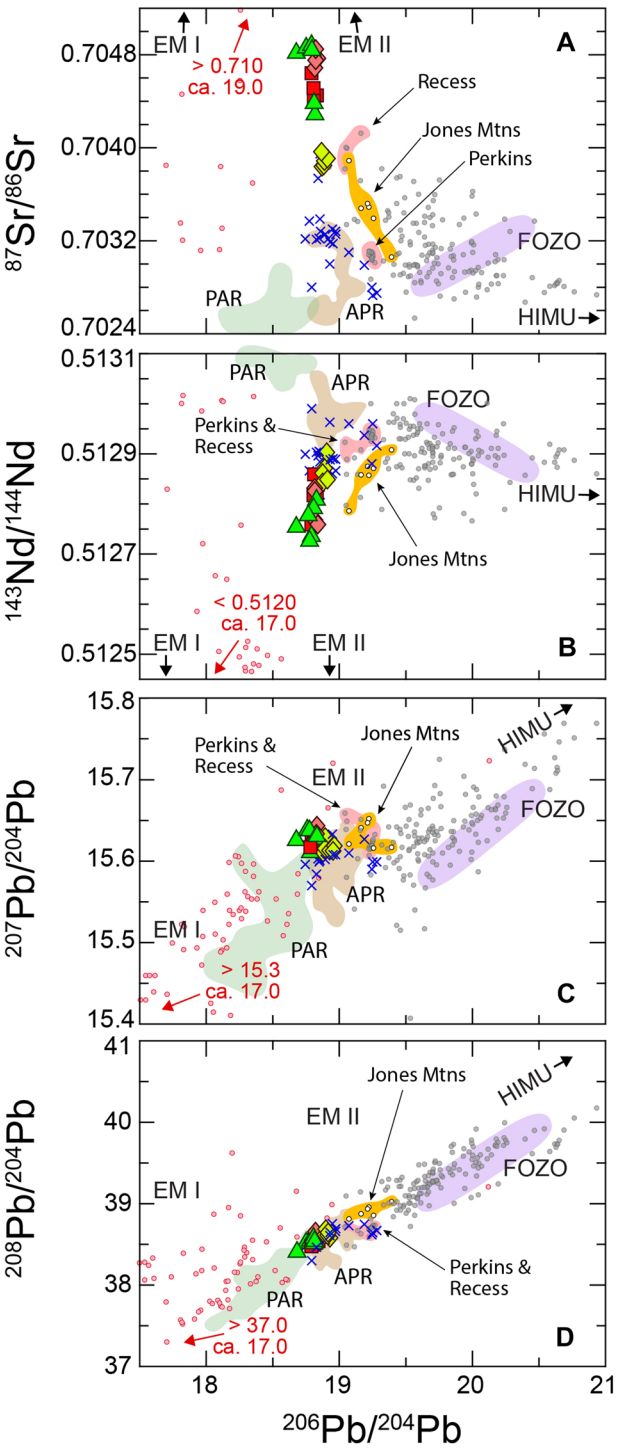

Fig. 6 Samples from Mount Early and Sheridan Bluff plotted on ▶ $^{206}Pb/^{204}Pb$ versus (**A**) $^{87}Sr/^{86}Sr$, (**B**) $^{143}Nd/^{144}Nd$, (**C**) $^{207}Pb/^{204}Pb$ and (**D**) $^{208}Pb/^{204}Pb$ ratio diagrams. In addition, shown are basaltic compositions (40–51 wt.% SiO_2) from the WARS and the Jurassic Karoo–Ferrar large igneous provinces (LIPs). All data are measured values (i.e., ratios have not been corrected for radiogenic in-growth). Data sources for WARS basalts, Miocene-Recent back-arc and post-subduction intraplate basalts from the Antarctic Peninsula and basalts from the Karoo–Ferrar LIPs are as in Figs. 2 and 3. Most samples of Karoo–Ferrar fall outside the X–Y scales for plots (**A**) and (**B**) and their general trend towards endmember compositions are shown by arrows and labeled values. Highlighted fields encompass basalts from the Jones Mountains (Hole et al. 1994; Hart et al. 1995) and Mount Perkins and Recess Nunatak in the Fosdick Mountains (Gaffney and Siddoway 2007; Panter et al. 2021b), which lie nearly 1500 km apart at the eastern (Jones) and western (Fosdick) extent of volcanism within the Marie Byrd Land Volcanic Group (Wilch et al. 2021). The positions of the mantle endmembers HIMU, DMM, EMI and EMII are from Hofmann (2007) and the field of FOZO (Hart et al. 1992) is based on the work of Stracke et al. (2005). The fields for mid-ocean ridge basalt (MORB) encompass 85 samples from the Pacific–Antarctic Ridge (PAR) compiled from Ferguson and Klein (1993); Vlastélic et al. (1998) and Hamelin et al. (2011) and 19 samples from the extinct Antarctic–Phoenix Ridge (APR) from Choi et al. (2008) and Haase et al. (2011)

on the origin of continental intraplate, monogenetic basaltic volcanism, worldwide (e.g., Moore et al. 1995; Jung and Masberg 1998; Lustrino et al. 2002; Brenna et al. 2010; Boyce et al. 2015). Determining the melt origin for volcanism in the USGVF is also of particular interest given the geographic novelty (i.e., isolated by more than 1000 km from any other known magmatism of Cenozoic age) and the enigmatic tectonic environment for volcanism (e.g., on the East Antarctic craton approximately 200 km inland from the Ross Sea boundary of the WARS).

Assessing magma differentiation processes

Fractional crystallization of olivine, clinopyroxene, plagioclase and titanomagnetite can explain much of the variation in major and trace element concentrations shown by Mount Early and Sheridan Bluff samples (Fig. 7A–C; Table S3). The range in olivine tholeiite compositions from Sheridan Bluff is predicted by thermodynamically based models as being controlled primarily by the crystallization of olivine and spinel (i.e., magnetite–ulvöspinel) under pressure conditions of less than 500 MPa and water contents ≤ 1 wt.% (Fig. 7C; also refer to Panter et al. 2021a, Fig. 10). Panter et al. (2021a) concluded, and it is re-affirmed here, that alkaline compositions (i.e., hawaiite and mugearite) cannot be produced by crystal fractionation of tholeiitic magmas. Contamination of tholeiitic magmas by average upper continental crust (Rudnick and Gao, 2003) also fails to explain the geochemistry of coexisting hawaiite lavas at Sheridan Bluff (see Panter et al. 2021a, Fig. 11).

Here, we advance our assessment of differentiation mechanisms using mass- and energy-balanced models (Bohrson et al. 2020; Heinonen et al. 2020) for the combined assimilation–fractional crystallization (AFC) process and taking into account our new isotopic data (Figs. 7 and 8, Table S4). For potential contaminants, we have selected samples from the Granite Harbour Intrusive complex, which is a group of Cambrian–Ordovician age calc-alkaline batholiths that

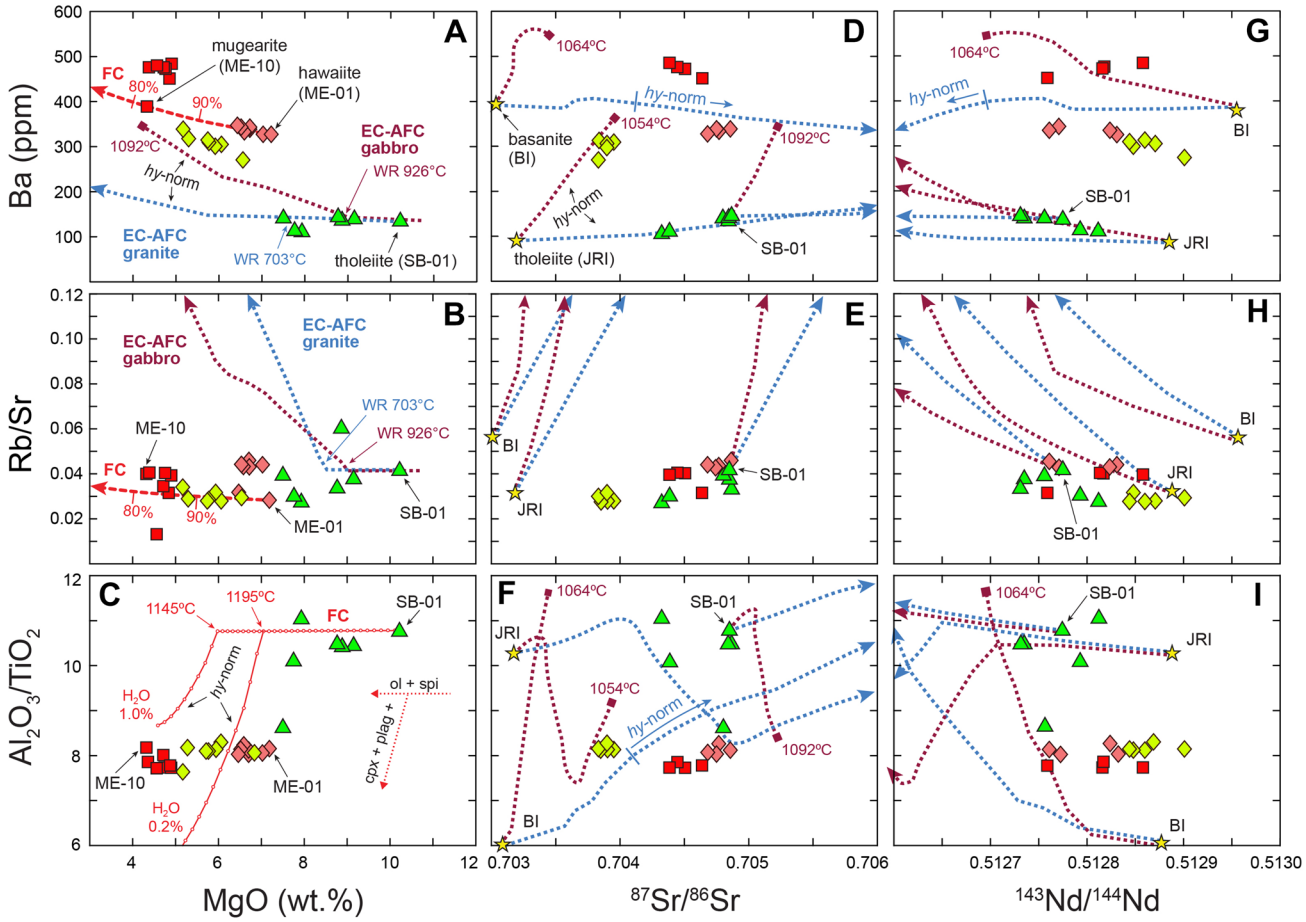

Fig. 7 Model curves for fractional crystallization (FC) and energy-constrained assimilation-fractional crystallization (EC-AFC) are evaluated relative to compositional variations of Mount Early and Sheridan Bluff samples. In plots (**A**–**C**), models for fractional crystallization are shown for one of the least differentiated hawaiite samples (ME15-001, abbreviated ME-01) at Mount Early and one of the least differentiated samples of olivine tholeiite (SB15-001, hereafter abbreviated SB-01) at Sheridan Bluff (Table 2). The crystallization trajectory from hawaiite (ME-01) in plots (**A**–**B**) and the relatively flat distribution of sample compositions between ME-1 and ME-10 in plot (**C**) are predicted by the least-squares (after Arth 1976) and Rayleigh distillation models that require removal of 7.8% olivine, 4.8% clinopyroxene, 5.6% plagioclase and 0.3% magnetite (Table S3). The bulk partition coefficients used are 0.18 for Ba, 0.03 for Rb, 0.57 for Sr (Table S3) and MgO is set at 3.5. Curves in plot (**C**), are for fractional crystallization of olivine tholeiite SB-01 calculated using the MELTS algorithm (Ghirorso and Sack 1995) over the temperature interval from of 1325° (temperature above the liquidus) to 1100 °C (using steps of 5 °C), a pressure interval of 500 MPa to 50 MPa (using steps of 25 MPa), a *f*O2 buffer equal to FMQ and a H_2O content of 1 wt.% and 0.20 wt.%. The initial conditions were set based on thermobarometric estimates for clinopyroxene–whole rock, olivine–whole rock and magnetite–ilmenite pairs (Reindel, 2018; Li, 2020). The temperatures of 1145 °C and 1195 °C mark inflections caused by the fractionation of plagioclase and clinopyroxene. Olivine and spinel (magnetite–ulvöspinel) remained on the liquidus over the entire temperature interval and the liquid is silica-saturated [CIPW normative hypersthene, abbreviated *hy*-norm]. For the model at 0.20 wt.% H_2O, orthopyroxene (not observed in samples) is on the liquidus only at temperatures between 1300° and 1270 °C (500 to 430 MPa). Energy and mass balance models of assimilation and fractional crystallization (Bohrson et al., 2020; Heinonen et al., 2020) in plots (**A**) and (**B**) predict relatively constant Ba concentrations and Rb/Sr ratios with decreasing MgO wt.% for Sheridan Bluff tholeiite over the FC portion of the run and increase when EC-AFC of wall rock (WR) commences at temperatures above the solidi of gabbro (926 °C) and granite (703 °C). Representative gabbro and granite compositions are from the Cambrian–Ordovician Granite Harbor Intrusive Complex (Dallai et al. 2003; Goodge et al. 2012). The same contaminants are used in plots (**D**–**I**) and, in addition to tholeiite from Sheridan Bluff, tholeiite from James Ross Island (JRI), Antarctic Peninsula (Košler et al. 2009) and an oceanic basanite from Sabrina Island (Hart 1988), Balleny Islands (BI), are used as proxies for 'uncontaminated' parental magmas. End-of-run temperatures labeled at the termini of EC-AFC gabbro curves are values close to thermal equilibrium between magma and wall rock. In addition, shown on EC-AFC granite model curves from basanite (BI) is the point at which the liquid becomes saturated with respect to silica (*hy*-norm). All liquids modeled along AFC curves from tholeiite are silica-saturated and can become silica-oversaturated towards end-of-run. The $^{87}Sr/^{86}Sr$ and $^{143}Nd/^{144}Nd$ ratios of basalts in plots (**D**–**I**) are not corrected for radiogenic ingrowth nor are the contaminants, which plot off-scale at much higher and lower ratios, respectfully. EC-AFC model parameters and inputs are provided in supplementary Table S4

comprise the basement rocks of the Transantarctic Mountains. Granite Harbour plutons are identified in outcrops over a distance of over 2500 km from northern Victoria Land to the southern Transantarctic Mountains (Encarnación and Grunow 1996; Goodge 2020) and are exposed within the upper Scott Glacier region (Doumani and Minshew 1965; Fitzgerald and Stump 1997). Wall-rock assimilation of granite (Goodge et al. 2012) and gabbro (Dallai et al. 2003) is modeled using Sheridan Bluff tholeiite and tholeiite from James Ross Island, Antarctic Peninsula (Košler et al. 2009) and basanite from Sabrina Island (Hart 1988), Balleny Islands (Fig. 1). The basalts were selected as proxies for magmas that have not been contaminated by continental crust. We acknowledge the geographic dissociation of these magmas from the USGVF but justify their selection based on (1) the geochemical similarity between tholeiite from James Ross Island and tholeiite from Sheridan Bluff that imply similar origins (discussed below) and because Cenozoic tholeiite associated with the WARS, which are extremely rare, have limited compositional data available (Panter et al. 2021b), and (2) that basanite from the Balleny Islands may represent a derivative from what could be ambient convective mantle beneath the southern Transantarctic Mountains. Hart et al. (1992) used Balleny Island basalt to help define the isotopic signature of the FOZO mantle endmember which has since been redefined by Stracke et al. (2005) and is shown in Fig. 6. Stracke et al. (2005) concluded that FOZO is a ubiquitous small-scale component in sources for MORB and is likely found throughout the entire mantle. Castillo (2015), on the other hand, proposed that FOZO is previously subducted oceanic lithospheric mantle and, hence, represents older, uppermost sections of MORB sources; such sources are inherently heterogeneous to begin with as they contain small-scale enriched components. Panter and Martin (2021) suggested that either a MORB−FOZO source mixture (*cf.* Stracke et al. 2005) or FOZO domains (*cf.* Castillo 2015) can account for most of the isotopic variation measured in basalts from the Ross Sea region of the WARS.

First, it is important to point out that Sr and Nd isotopes of Mount Early and Sheridan Bluff samples are less enriched (i.e., having lower $^{87}Sr/^{86}Sr$ and higher $^{143}Nd/^{144}Nd$) in the more evolved compositions relative to the least fractionated compositions, making it difficult to explain by AFC. Specifically, olivine tholeiite sample SB15-001, which is one of the most mafic samples (highest concentrations in MgO, Cr and Ni) and one of the most enriched isotopically (i.e., low Nd and high Sr isotope values), cannot be parental to the whole of the Mount Early and Sheridan Bluff suite. Furthermore, the relatively invariant major and trace element concentrations of tholeiites with decreasing MgO content (Figs. 3A and 7A; also refer to Figs. 6 and 7 in Panter et al. 2021a) is distinctive from trends in alkaline compositions. In other words, the data does not show smooth trends between subalkaline and alkaline types which would be expected if they were related along a single liquid line of decent from a common parent by AFC or fractional crystallization processes.

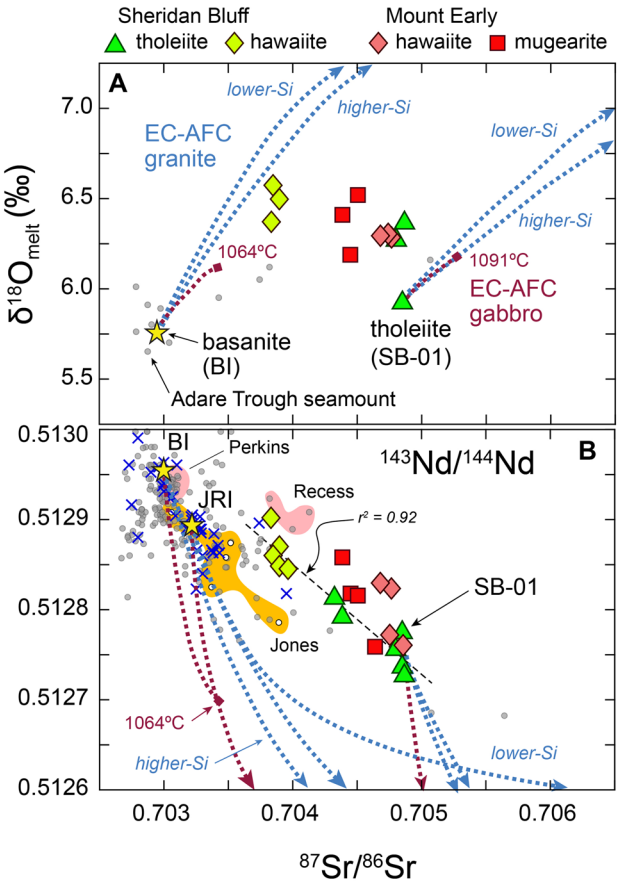

Fig. 8 Measured $^{87}Sr/^{86}Sr$ versus $\delta^{18}O_{melt}$ from olivine (**A**) and $^{143}Nd/^{144}Nd$ of Mount Early and Sheridan Bluff compositions compared with WARS basalts from the northwestern Ross Sea region and include seamounts in the Adare Basin and Trough (Krans 2013; Panter et al. 2018) and in (**B**) also include back-arc and post-subduction intraplate basalts from the Antarctic Peninsula along with basalts from Mount Perkins and Recess Nunatak (Fosdick Mountains) and Jones Mountains. Symbols and data sources are the same as previous figures. The $\delta^{18}O_{melt}$ is calculated using the Eq. $10^3 \ln\alpha_{olivine-basalt} = A \times 10^6/T^2$, in which A is -1.77 (Zhao and Zheng, 2003) and for T (kelvin) is the olivine crystallization temperature determined by olivine thermometry listed in Table 1 following the method of Putirka et al. (2007) and Putirka (2008). A summary of olivine thermometry is provided in Table S5. For samples whose olivine crystallization temperatures could not be determined melt values were calculated using an average olivine-melt fractionation of 0.80 (Table 1). Contaminants used for thermodynamically constrained AFC modeling (EC-AFC) are the same as in Fig. 7 with the addition of granite processing a higher SiO_2 content (c. 74 wt.%) relative to *lower*-Si granite (c. 68 wt.%). $\delta^{18}O$ for gabbro (7‰) and granites (12‰) used in EC-AFC models are based on whole rock values (Dallai et al. 2003). EC-AFC model parameters are provided in supplementary Table S5. A regression of the data for coexisting and contemporaneous Sheridan Bluff hawaiite and tholeiite lavas shows a very strong linear relationship ($r^2 = 0.92$)

The contamination of tholeiite by granite or gabbro cannot explain either the compositional variations within the tholeiite suite or the derivation of alkaline compositions (Fig. 7). Models for the assimilation of granite by tholeiite from James Ross Island have some success in emulating variations in $^{87}Sr/^{86}Sr$ and $^{143}Nd/^{144}Nd$ with Ba content (Fig. 7D and G) and $^{143}Nd/^{144}Nd$ with Al_2O_3/TiO_2 ratios (Fig. 7I) but cannot account for the relatively flat compositional arrays shown on Rb/Sr ratio plots (Fig. 7E and H). EC-AFC models using basanite are also somewhat successful in predicting the variation in $^{143}Nd/^{144}Nd$ ratios with Ba content for silica-undersaturated alkaline compositions (Fig. 7G) but fail in other cases, particularly because the calculated liquids become silica-saturated (i.e., hypersthene-normative) during the assimilation of granite (Fig. 7D and F).

Magmatic differentiation by AFC for Mount Early and Sheridan Bluff samples is also evaluated on plots of $^{87}Sr/^{86}Sr$ ratios versus $\delta^{18}O_{melt}$ and $^{143}Nd/^{144}Nd$ ratios. In Fig. 8, samples are compared to WARS basalts, including oceanic intraplate basalts from the Antarctic Plate (i.e., Balleny Islands and Adare Basin and Trough), and back-arc and post-subduction intraplate basalts from the Antarctic Peninsula. The overall trend of Mount Early and Sheridan Bluff samples on these plots is opposite of what is predicted by the EC-AFC models (i.e., more evolved samples have higher $^{143}Nd/^{144}Nd$ ratios and oxygen isotope values but lower Sr isotope values than the less evolved samples). It is possible that selection of different parental magmas and different contaminants could account for the isotopic signatures of individual sample groupings. But again, it is unlikely, even with special pleading, that a single liquid line of decent by AFC could produce hawaiite from tholeiite and explain the uninterrupted lava sequence of these compositional types at Sheridan Bluff.

In summary, we have tested for crustal assimilation using a variety of potential contaminants as well as alternative parental magmas to account for the geochemical and isotopic characteristics of Mount Early and Sheridan Bluff samples. The results suggest that AFC is not the process regulating magma differentiation or the origin of their isotopic compositions. Therefore, we now turn our attention to source inheritance and melt generation processes.

Mantle partial melting and source heterogeneity

We have established that the relationship between tholeiite and alkaline magmas cannot be explained by crystal fractionation or AFC, and therefore, their association must be a result of differences in the conditions and source heterogeneity of their origination. Changes in the degree of mantle partial melting is often used to explain the coexistence of tholeiite and alkaline compositions (e.g., Jung and Masberg 1998; Wanless et al. 2006; Boyce et al. 2015; Kocaarlson et al. 2018) and was modeled by Panter et al. (2021a) to account for the origin of the two magma types at Sheridan Bluff. Here we re-evaluate their models. Like the previous study our estimates indicate that tholeiitic melts can be generated by higher degrees of partial melting (c. 5−6%, Fig. 9A and B) relative to alkaline melts (c. 1.5−2%, Fig. 9A) and that garnet is residual in the source of both types. This helps to explain their similar HREE and Y concentrations but disparate abundances in highly incompatible trace elements as featured on mantle normalized multi-element diagrams (e.g., Fig. 9C). But unlike the melting results of Panter et al. (2021a), which resulted in an unrealistically high estimate of partial melting to generate tholeiite (20%) from a homogenous source (i.e., same mineral mode and melt proportions as what was used for alkaline melt), the preferred source mode for tholeiite has a higher proportion of clinopyroxene (27% vs. 15%), less garnet (2% vs. 4%) and does not contain amphibole. The source of alkaline compositions on the other hand may contain amphibole and hawaiite samples are better matched by melt models that use modes of 4–5% amphibole with melt proportions of c. 50% (curves labeled 2 and 3 in Fig. 9A). Amphibole, along with garnet, would contribute to the higher Nb/Y ratio of hawaiite relative to tholeiite (Fig. 9A). High Nb concentrations (30 to ≥ 100 PUM; McDonough and Sun 1995) have been measured on vein and disseminated amphibole in peridotite and hornblendite (Ionov and Hofmann 1995; Ionov et al. 1997; Moine et al. 2001), including within xenoliths of lithospheric mantle brought to the surface by alkaline magmas within the WARS (Coltorti et al. 2004; Perinelli et al. 2006, 2017). In addition, the compatibility of Nb in amphibole is mostly less than unity while Y is compatible ($D^{amph/melt} = 0.53$ and 1.48, respectively; averaged values calculated by Pilet et al. 2011 using data from Tiepolo et al. 2000a, 2000b, and 2007). Furthermore, Pilet et al. (2008) found that melting of amphibole-rich metasomatic veins [hornblendite (Fig. 9A) and clinopyroxene hornblendite] at upper mantle conditions (1.5 GPa, ~ 1150 °C) produce liquids with high K/Rb (> 800−1600) and Ba/Rb (> 30−60) ratios and moderate to low Zr/Nb (≤ 5) ratios. The least fractionated hawaiite samples (ME15-001 and SB15-006, Table S1) have higher K/Rb (> 600) and Ba/Rb (12−15) ratios relative to the least fractionated tholeiites (< 400 and < 9, respectively; SB15-001 and SB15-002) and lower Zr/Nb ratios (c. 5 versus c. 9 for tholeiite), which support contribution from amphibole in the source of alkaline magmas at Mount Early and Sheridan Bluff. Given the low TiO_2 concentrations measured in both alkaline and subalkaline compositions (Fig. 3B) it is unlikely that phlogopite, if present, played a significant role in source melting.

Lastly, differences in primary source compositions for alkaline and tholeiite lavas at Sheridan Bluff are also

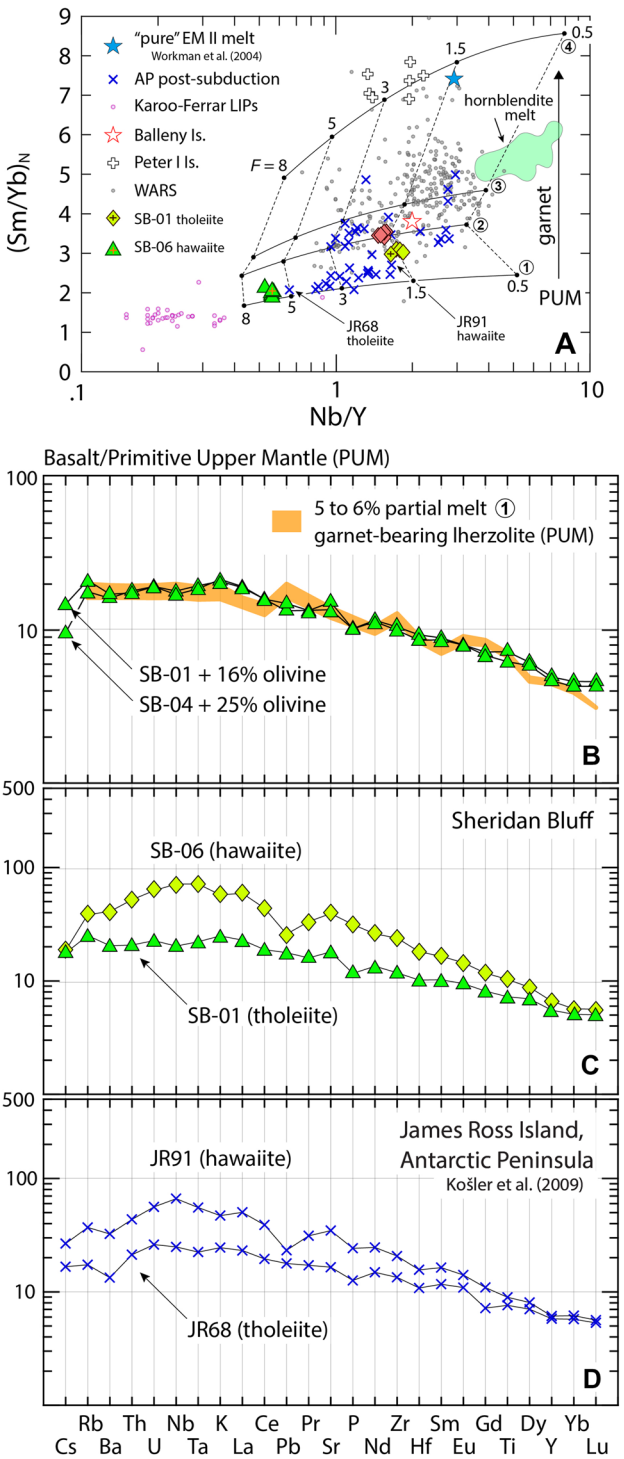

Fig. 9 (**A**) plot of trace element chemistry of mafic samples (≥5 wt.% MgO and ≤52 wt.% SiO_2) and partial melting model curves on a Nb/Y versus $(Sm/Yb)_N$ diagram. Mineral mode and melt proportion are adapted from Ersoy et al. (2010) for non-modal batch melting (Shaw, 1970) of primitive upper mantle (PUM; McDonough and Sun, 1995) are: (1) garnet-bearing lherzolite = Ol $_{53(0.05)}$ + Opx $_{18(0.05)}$ + Cpx $_{27(0.81)}$ + Grt $_{2(0.09)}$; (2) garnet- and amphibole-bearing lherzolite = Ol $_{55(0.05)}$ + Opx $_{22(0.05)}$ + Cpx $_{15(0.40)}$ + Grt $_{3(0.05)}$ + Amp $_{5(0.45)}$; (3) amphibole- and garnet-bearing lherzolite = Ol $_{55(0.05)}$ + Opx $_{22(0.05)}$ + Cpx $_{15(0.40)}$ + Grt $_{4(0.05)}$ + Amp $_{4(0.50)}$; (4) garnet lherzolite = Ol $_{55(0.05)}$ + Opx $_{22(0.05)}$ + Cpx $_{15(0.81)}$ + Grt $_{8(0.09)}$. Partition coefficients used are from Ersoy et al. (2010 and references therein). The amount of partial melt (*F*) on model curves ranges from 8.0 to 0.5%. Data sources and constraints for WARS basalts and back-arc and post-subduction intraplate basalts from the Antarctic Peninsula are the same as in Fig. 2. Data sources and constraints for Karoo–Ferrar (low-Ti) basalts are the same as in Fig. 3 and for the basalt from the Balleny Islands (Sabrina Island) is provided in Fig. 8. Subaerial basalts from Peter I Island (Bellingshausen Sea) are from Prestvik et al. (1990), Hart et al. (1995) and Kipf et al. (2014). The field labeled "hornblendite melt" encompassing compositions that were derived from experiments by Pilet et al. (2008) on natural hornblendite (AG4) fused at a pressure of 1.5 GPa and at temperatures that ranged from 1150° to 1350 °C (~solidus to ~liquidus). (**B–D**) PUM-normalized multi-element plots of basalts and melt compositions. (**B**) tholeiite samples from Sheridan Bluff are corrected for fractionation of olivine by first normalizing major elements to Mg# 73. This was accomplished by adding olivine, incrementally, to each composition while maintaining a constant Fe^{2+}/Mg K_D value equal to 0.30 until the Mg# reached 73 and olivine reached Fo90. Trace element concentrations were reduced by the percentage of olivine that was added back to each composition. The olivine corrected samples are compared to compositions derived from 5 to 6% partial melt of a garnet-bearing lherzolite [model (1)]. Plots (**C** and **D**) compare hawaiite and tholeiite samples from Sheridan Bluff with similar compositions of mafic back-arc alkaline and tholeiite from James Ross Island, Antarctic Peninsula (Košler et al., 2009)

inferred based on their Ce/Pb and Nb/U ratios, which is revealed graphically in trace element patterns (Fig. 9C). Olivine tholeiite sample SB15-001 has Ce/Pb and Nb/U ratios of 12 and 29, respectively, while hawaiite sample SB15-006 has ratios of 19 and 37, respectively. Overall, these ratios are at the lower range of oceanic basalts [e.g., for MORB and non-EM II-type OIBs the Ce/Pb ratios = 25 ± 5, Hofmann et al. (1986) and Nb/U ratios = 47 ± 10–11, Sims and DePaolo (1997); Hofmann (2003)].

In summary, the variations in radiogenic isotopes (Fig. 6A and B) along with differences in trace element ratios between alkaline and subalkaline types indicate modal and compositional heterogeneity in the mantle beneath these volcanoes. Since olivine tholeiite and hawaiite lavas were erupted contemporaneously and likely from a single vent at Sheridan Bluff (Smellie and Panter 2021), the compositional heterogeneities must be at an extremely small scale.

Coexisting subalkaline and alkaline volcanism in West Antarctica

Intraplate basaltic volcanism in West Antarctica is expressed in numerous volcanic field consisting of monogenetic cones (LeMasurier and Thomson 1990; Smellie et al. 2021a). However, the occurrence of tholeiite compositions are

rare (Fig. 2, inset) and are found in small volumes along with mafic alkaline compositions in the Jones Mountains (Hole et al. 1994; Hart et al. 1995), western Ellsworth Land (Fig. 1), which is the easternmost volcanic field of the Marie Byrd Land Volcanic Group (Wilch et al. 2021; Panter et al. 2021b). A single isolated outcrop of tholeiitic basalt is found in the Fosdick Mountains in western Marie Byrd Land (Fig. 1) and other basalts within 10–20 km range from strongly silica-undersaturated (c. 13% nepheline-normative) basanite at Recess Nunatak to alkali basalts at Mount Perkins, which vary from weakly silica-undersaturated (c. 1% nepheline-normative) to silica-saturated (1–6% hypersthene-normative) compositions (Gaffney and Siddoway 2007; Panter et al. 2021b). The close association of tholeiite and alkaline volcanism also occurs along the north-eastern coast of the Antarctic Peninsula at Seal Nunataks and on James Ross Island (Fig. 1) (Smellie 1987; Hole 1990; Hole et al. 1993a; Košler et al. 2009). Like Sheridan Bluff, both compositional types are found within a single edifice at Bruce Nunatak (Seal Nunataks) and coexist in close proximity (< 10 km) elsewhere. Olivine tholeiite and hawaiite from Sheridan Bluff have remarkably similar trace element abundances as those from the Ulu Peninsula on James Ross Island (Fig. 9C and D), which implies origins from similar mantle sources and melting under similar conditions. An additional shared trait is that tholeiitic basalts that have been measured commonly have higher $^{87}Sr/^{86}Sr$ values than alkaline basalts. Strontium isotopic ratios of tholeiite at Sheridan Bluff are higher (0.70432−0.70487) than hawaiite (0.70383−0.70395; Table 2). In the Jones Mountains, the highest Sr isotope value measured by Hart et al. (1995) is for tholeiite (0.70389, sample 69-C-15) and the lowest is for basanite (0.70306, sample 69-C-12). These lavas were collected within 10 km of each other and were deposited 1 to 3 m above a regional erosional unconformity (Craddock et al. 1964; and notes of C. Craddock from the U.S. Polar Rock Repository database https://prr.osu.edu/), and although the duration of volcanism in the Jones Mountains is poorly constrained (Rutford and McIntosh 2007), the field relationships suggest that they are of similar age. At the Seal Nunataks, Antarctic Peninsula, Hole (1990) reports higher Sr isotope values in tholeiite (> 0.7032) relative to alkaline compositions (< 0.7032). Specifically, at Bruce Nunatak, the Sr isotope value of tholeiite is 0.70329 while the coexisting hawaiite is lower at 0.70307, which again broadly mimic differences in the Sr isotopes measured at Sheridan Bluff. These rare, closely associated alkaline−subalkaline systems in West Antarctica indicate mantle source heterogeneity that is similar in scale to what must exist beneath Sheridan Bluff and may imply similar conditions for melting (discussed as follows).

Mantle source types

It is apparent from the trends in isotopic data plotted in Figs. 6 and 8 that at least two distinct source components; one relatively enriched and one more depleted, were involved in the petrogenesis of Sheridan Bluff and Mount Early magmas. In addition, that Mount Early had a more homogeneous source relative to Sheridan Bluff, which implies another length-scale in mantle heterogeneity. The basaltic compositions form arrays that extend towards enriched (i.e., high Sr and low Nd isotope values) mantle sources, mainly towards the EM II-type (Fig. 6A and B). The mildly ^{18}O-enriched signature of olivine (Fig. 5, Table 1) along with elevated $^{87}Sr/^{86}Sr$ values (Fig. 8A) approach values of ocean island basalts (OIB) derived from mantle sources containing EM II material (Eiler 2001; Eiler et al. 1997; Workman et al. 2004; 2008; Jackson et al. 2007). However, it is unlikely that the enriched component in Mount Early and Sheridan Bluff compositions are from an oceanic EM II source but instead appear to be closely related to a mantle source that supplied Jurassic Ferrar−Karoo magmatism. This could explain their shared geochemical characteristics such as the sub-parallel trends at low TiO_2 concentrations (Fig. 3B), low FeO^T contents (Fig. 3A) and for Sheridan tholeiite, low Nb/Y ratios (Fig. 9A).

For the more depleted endmember component (i.e., lower Sr and higher Nd isotope values, Fig. 6A and B), we have shown that mafic compositions at Mount Early and Sheridan Bluff share many geochemical and isotopic characteristics with Miocene-Recent alkaline (and rare tholeiitic) basalts from the Antarctic Peninsula. Notably they have similar, relatively un-radiogenic Pb isotopic signatures as well as major and trace element abundances which are markedly different from most WARS basalts (Fig. 10). Close exceptions are the basalts from the Jones Mountains and the Fosdick Mountains (Figs. 6 and 10). These basalts have similar $^{206}Pb/^{204}Pb$ (Fig. 10A and B) and $^{207}Pb/^{204}Pb$ (not shown) ratios and lower $^{208}Pb/^{204}Pb$ ratios (Fig. 10C and D) giving them a closer compositional affinity to Sheridan Bluff and Mount Early basalts (plus tholeiite and alkaline basalts from the Antarctic Peninsula) than basalts from the rest of the WARS (Fig. 10).

Antarctic Peninsula back-arc and post-subduction intraplate basalts have been ascribed to a mantle source for enriched MORB (E-MORB; Hole et al. 1993a; Hole 2021) or a mixture of mantle sources that produce MORB and EM II (Košler et al. 2009) basalts. However, in a recent study, Haase and Beier (2021) concluded that volcanism at James Ross Island was not MORB-sourced. This is based, primarily, on the trend of $^{206}Pb/^{204}Pb$ versus $^{208}Pb/^{204}Pb$ sample values that parallel but plot above the MORB field defined by compositions from the East Pacific Rise. However, when

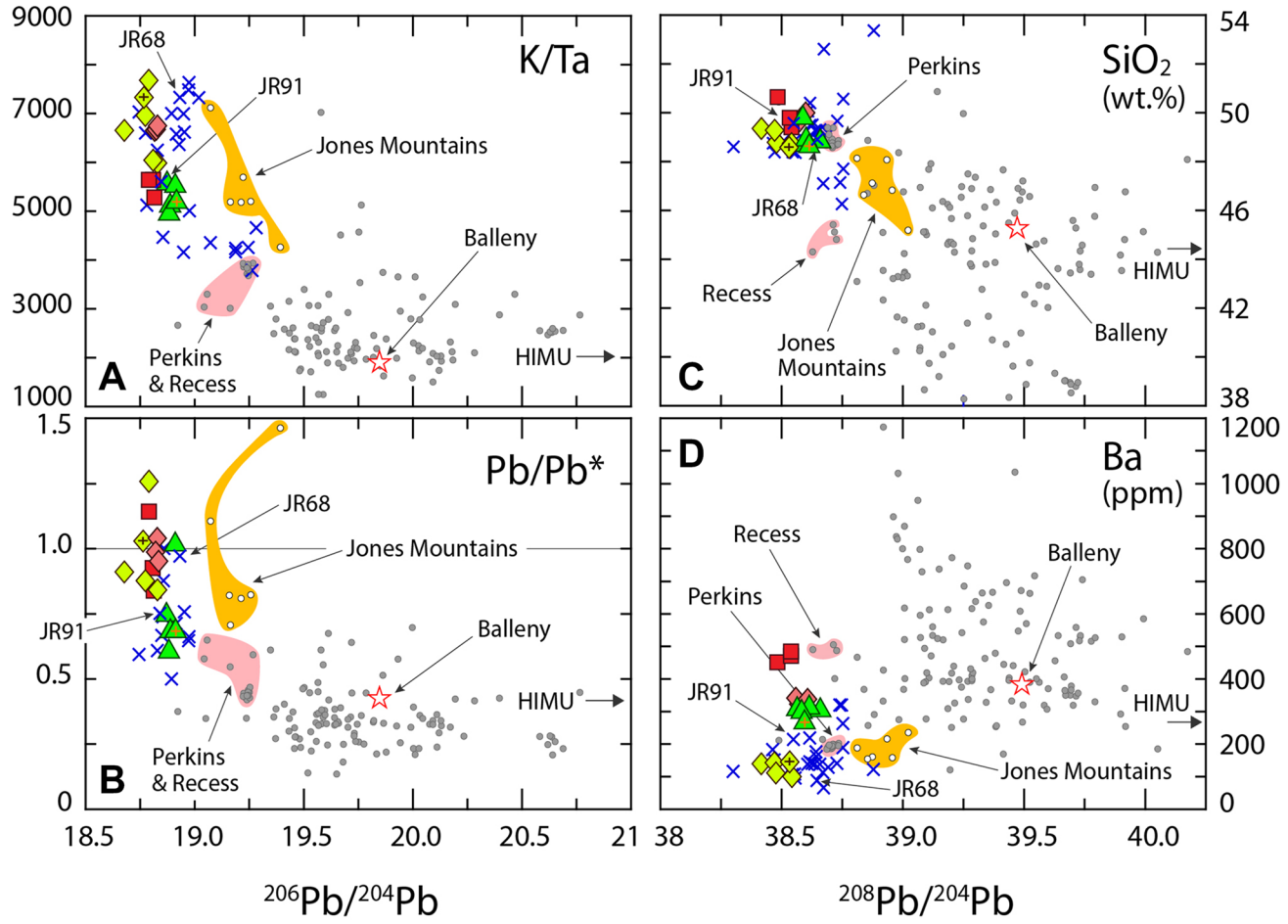

Fig. 10 Plots of Pb isotopic ratios $^{206}Pb/^{204}Pb$ and $^{208}Pb/^{204}Pb$ versus (**A**) K/Ta and (**B**) Pb/Pb* ratios and (**C**) SiO_2 (wt.%) and (**D**) Ba (ppm), respectively. $Pb/Pb^* = Pb_N/\sqrt{(Ce_N \times Pr_N}$, where values c. 1.0 represent a linear alignment of Ce−Pb−Pr on mantle normalized multi-element plots (e.g., refer to the pattern for sample SB-01 shown in Fig. 9C). Samples from Mount Early and Sheridan Bluff are compared with basalts (MgO ≥ 4.7 wt.%) from West Antarctica that include back-arc basalts from James Ross Island on the Antarctic Peninsula (samples JR68 and JR91 shown in Fig. 9D are indicated) and WARS samples (data sources are given in Fig. 2). Symbols for Sheridan Bluff tholeiite sample SB15-001 and hawaiite sample SB15-006 (abbreviated SB-01 and SB-06) are the same as used in Fig. 9A. Basalt from Sabrina Island (Balleny islands; Johnson et al. 1982; Hart 1988) is also shown for comparison [note that in plot (**B**) the Pb/Pb* ratio of this sample is approximated using Sr (or Nd) in place of Pr (not measured)]. The composition of HIMU is based on basalt samples from Mangaia in the Austral-Cook island group (compiled from the GEOROC database; available at http://georoc.mpch-mainz.gwdg.de/)

back-arc and post-subduction basalts, including those from James Ross Island, are compared to MORB samples from the active Pacific–Antarctic Ridge (PAR) in Pb–Pb isotope space (Fig. 6C and D) they cluster together with those from Mount Early and Sheridan Bluff near the most radiogenic end. They also overlap with MORB samples from the extinct Antarctic–Phoenix Ridge (APR). Basalts from the Jones and Fosdick mountains have slightly more radiogenic values for Pb isotopes (Fig. 10) and their sources have been constrained by comparison with both Antarctic Peninsula and WARS volcanism (Hole et al. 1994; Hart et al. 1995; Gaffney and Siddoway 2007; Panter et al. 2021b). Overall, their geochemical affinity matches the broad characteristics of OIB but the Pb isotopes are not HIMU-like (i.e., derived from mantle sources that have high $\mu = {}^{238}U/{}^{204}Pb_{t=0}$ ratios promoting high $^{206}Pb/^{204}Pb$ ratios with time), which is a pervasive component in WARS volcanism (Panter 2021a, b and references therein). Their Pb isotopic values suggest a greater contribution from more depleted mantle (i.e., source of E-MORB) that is similar to sources for back-arc and post-subduction basalts from the Antarctic Peninsula and what also appears to be a major source component in Sheridan Bluff and Mount Early basalts of the USGVF.

Origin of mantle sources and contributions to USGVF volcanism

The close compositional affinity of mafic volcanism at Mount Early and Sheridan Bluff with basalts from the Antarctic Peninsula and from the two volcanic fields within the Marie Byrd Land Volcanic Group (i.e., Jones and Fosdick mountains) warrant an appraisal of their mantle legacies as possible analogues. Back-arc and post-subduction intraplate volcanism on the Antarctic Peninsula have been ascribed to slab rollback and slab-window tectonics, respectively, that promoted decompression melting of asthenosphere with only minor contributions from subduction-modified lithospheric mantle (Hole 1988; Hole et al. 1993a; Košler et al. 2009). Alternatively, Hole (2021) proposed that partial melting of slab-hosted pyroxenite can produce their geochemical characteristics. The interpretation of the mantle origin of the Jones Mountains is also debated. Hole et al. (1994) invoked a mantle plume ('Marie Byrd Land plume'; LeMasurier and Rex 1989; Hole and LeMasurier 1994) that migrated radially outward from central Marie Byrd Land to trigger melting in western Ellsworth Land. Hart et al. (1995) on the other hand, implicated both sub-lithospheric (EM II-like 'Peter I plume') and lithospheric mantle sources for volcanism with decompression melting being initiated by rifting. Hart et al. (1995) further suggested that, in the Mesozoic, the continental lithosphere along the proto-Pacific Gondwana margin was modified by subduction zone processes to explain the low Pb isotopic signatures and the low Ce/Pb ratios (*cf*. high Pb/Pb* ratios in Fig. 10) of the basalts in the Jones Mountains. The high and broad range in K/Ta and Pb/Pb* ratios mimic those of back-arc and post-subduction basalts from the Antarctic Peninsula (Fig. 10A and B) and further strengthen the argument for subduction zone influence on melt sources for intraplate basalts (e.g., Nakamura et al. 1985; Rogers et al. 1987; Demény et al. 2012; Zhao et al. 2021). For volcanism in the Fosdick Mountains, Gaffney and Siddoway (2007) suggested a mantle source that is locally heterogenous and not sampled by other volcanoes in the Marie Byrd Land province. They conclude that mixing between melts of subducted oceanic crust and continental lithospheric mantle; mantle that was previously metasomatized by subduction-related fluids, could explain the range in basalt compositions. But the question remains; are any of these mantle types appropriate as sources for the USGVF volcanism?

The case for subduction zone influences on the composition of mantle sources for Cenozoic volcanism is a causatum of the fact that subduction dominated the tectonic regime episodically from the Neoproterozoic to the Late Cretaceous along the pre-dispersal length of the Pan-Pacific margin of the Gondwana (Cawood 2005; Nelson and Cottle 2017) and it is likely that sinking slab material still exists beneath the continent (Bredow et al. 2021). The convergent tectonic regime included the formation of the southern Gondwanan subduction zone and magmatic arc that was synchronous with the initial phase of Jurassic break-up magmatism (Rapela et al. 2005). Subduction-modified subcontinental lithosphere has been proposed as a major source component for the Karoo–Ferrar LIPs (e.g., Hergt et al. 1991; Mozhan et al. 1996; Ivanov et al. 2017; Luttinen 2018; Choi et al. 2019; Elliot and Fleming 2021) and is likely to still exist in the mantle lithosphere beneath the upper Scott Glacier. Melting of this mantle type could contribute to the enriched compositional characteristics of Sheridan Bluff and Mount Early basalts.

The existence of a more depleted mantle source component (i.e., one that can produce E-MORB-like compositions) beneath Sheridan Bluff and Mount Early may also be related to pre-break-up plate dynamics that occurred along the Gondwanan margin. Luyendyk (1995) proposed that collision in the Late Cretaceous between the Pacific–Phoenix Ridge and the Gondwana continent triggered the rapid change from subduction to extension leading to the separation of Zealandia from Antarctica and the early development of the WARS. Ridge-trench collisions progressed to the east and northward until seafloor spreading ceased at around 3.3 Ma at the Antarctic–Phoenix Ridge (Larter and Barker 1991; Livermore et al. 2000; Haase et al. 2011). Since the break-up of Gondwana (c. 90 Ma) an early, broad phase of rifting is estimated to have resulted in 500 to 1000 km of crustal extension across the entire Ross Sea between Marie Byrd Land and the western boundary of the East Antarctica craton (DiVenere et al. 1994; Luyendyk et al. 1996) and was followed by a later period (c. 80–40 Ma) of more focused rifting in the western Ross Sea with an additional c. 300 km of extension (Molnar et al. 1975; Cande et al. 2000; Huerta and Harry 2007). We suggest that materials from the upper mantle (i.e., asthenosphere) and possibly remnants of Phoenix Plate were introduced to the region beneath the upper Scott Glacier when the Phoenix Ridge collided with the pre-extended Gondwanan margin in the Late Cretaceous.

Mixing of enriched and depleted mantle components

A simple mixture of an enriched mantle source and a more depleted mantle source may best explain the geochemical and isotopic characteristics of mafic samples from Mount Early and Sheridan Bluff. We evaluate this idea using basalts from the Antarctic–Phoenix Ridge and mafic intrusions from the Karoo (Fig. 11A). We estimate a mixture consisting of 50 to ≥ 60% of the enriched mantle component

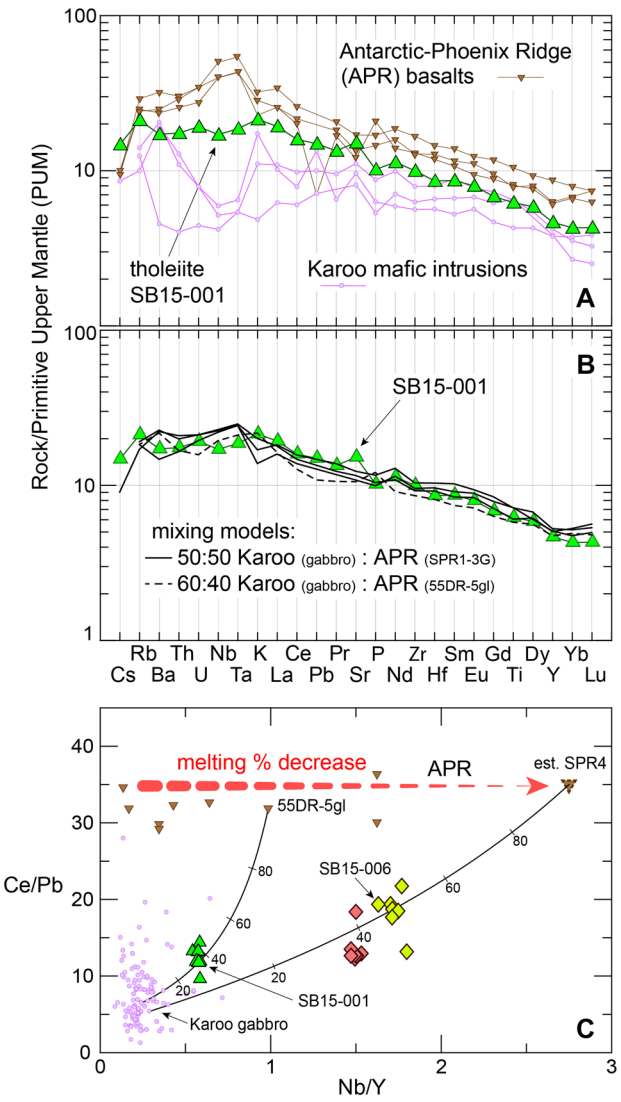

Fig. 11 Geochemical diagrams used to evaluate simple mixing between mafic melts derived from two different mantle source types (i.e., enriched metasomatized lithosphere and a more depleted asthenosphere) to explain mafic compositions at Sheridan Bluff and Mount Early. (**A**) Sheridan Bluff tholeiite (SB15-001, corrected for olivine fractionation, refer to Fig. 9 and caption) is compared with selected mafic compositions from the Antarctic–Phoenix Ridge (APR) and Karoo LIP, Dronning Maud Land on a primitive upper mantle (PUM) normalized (McDonough and Sun 1995) diagram. (**B**) simple mixing of gabbroic compositions from the Karoo (Luttinen et al., 2006; Sushchevskaya et al. 2009 Heinonen et al. 2010) in roughly equal proportions with basaltic glass from the ARP (Choe et al. 2007) provide a reasonable match to tholeiite sample SB15-001. (**C**) Ce/Pb versus Nb/Y ratio plot showing variations in Mount Early and Sheridan Bluff samples along with those from the APR (Haase et al. 2011) and Karoo–Ferrar LIPs (low-Ti compositions, refer to Fig. 3 caption for criteria and data sources). Simple mixing between APR basaltic glass (≤40% of sample 55DR-5gl) and Karoo gabbro (≥60% of sample SKV1500, Luttinen et al., 2006) is able to produce Ce/Pb and Nb/Y ratios of Sheridan Bluff tholeiite. The $^{87}Sr/^{86}Sr$ ratio of tholeiite sample SB15-001 (0.70485) can be re-produced by a 25:75 mix of these samples. To predict hawaiite from Sheridan Bluff requires an APR composition with higher Nb/Y ratios. The increase in Nb/Y ratios correlate with higher La/Sm and Ba/La ratios in APR samples that Choe et al. (2007) and Haase et al. (2011) interpret to be the result of lower degrees of partial melting of a heterogeneous source (i.e., low degree melts tapping a greater proportion of an enriched and fertile mantle source for E-MORB). Basalts dredged from an axial seamount in the P3 segment of the Antarctic–Pacific Ridge have Nb/Y ratios between 2 and 3 (SPR4 samples from Choe et al. 2007) but Pb concentrations are not reported. Assuming relatively constant Ce/Pb ratios for APR basalts we estimate an endmember composition ("est. APR) and mix that with Karoo *gabbro* (dolerite sample 47139–7, Sushchevskaya et al. 2009) to match Sheridan Bluff hawaiite (SB15-006) near to the proportions of 45:55. The $^{87}Sr/^{86}Sr$ value (0.70383) of Sheridan Bluff hawaiite (SB15-006) can be re-produced by a similar mixing proportion of 49% APR basalt (55DR-5gl) with 51% Karoo *gabbro* (47139–7)

(i.e., metasomatized lithosphere similar to the source for Karoo–Ferrar magmas) with the remainder being the more depleted mantle component (i.e., asthenosphere similar to the source for E-MORB compositions of the Antarctic–Phoenix Ridge) to best match tholeiite compositions (Fig. 11B). Proportionally, a mixture that has a larger contribution from an enriched mantle lithosphere and higher degree melts of depleted asthenosphere best match the lower Ce/Pb and Nb/Y ratios of tholeiite compositions while the alkaline compositions are matched by a mixture that has a larger contribution from asthenosphere but has melted to a lesser degree (Fig. 11C). A greater proportion of the more depleted mantle component can also explain why hawaiite lavas at Sheridan Bluff have lower Sr and higher Nd isotope values relative to the tholeiite lavas (Fig. 8B), which are contemporaneous and lie conformably below them. Furthermore, the strong linear and non-overlapping array of Sheridan Bluff samples in Sr–Nd isotope space support a progressive change in the proportions of the mantle source mixture during melting. Lastly, average $^{206}Pb/^{204}Pb$ and $^{208}Pb/^{204}Pb$ values for Sheridan Bluff hawaiite samples ($n=5$) are higher at 18.892 (±0.014, 2SSE) and 38.604 (±0.007), respectively, while lower average values for tholeiite samples ($n=6$) are 18.774 (±0.043) and 38.486 (±0.032), respectively (Fig. 6D and Table 2). This demonstrates that a greater proportion of the Ferrar–Karoo component is required for tholeiite compositions relative to hawaiite at Sheridan Bluff (Fig. 11C).

Cause of mantle melting

Further insight on the origin and mantle source domains for the USGVF can be advanced by an understanding of the mechanism for melting. Evidence for lithospheric detachment (aka. delamination or foundering) is provided by shear wave velocity (V_s) models (Fig. 12A) that reveal a low velocity zone beneath the southern Transantarctic Mountains at a depth of between 50 and 80 km (Heezel et al. 2016; Shen et al. 2018). The slowest V_s is centered beneath the USGVF

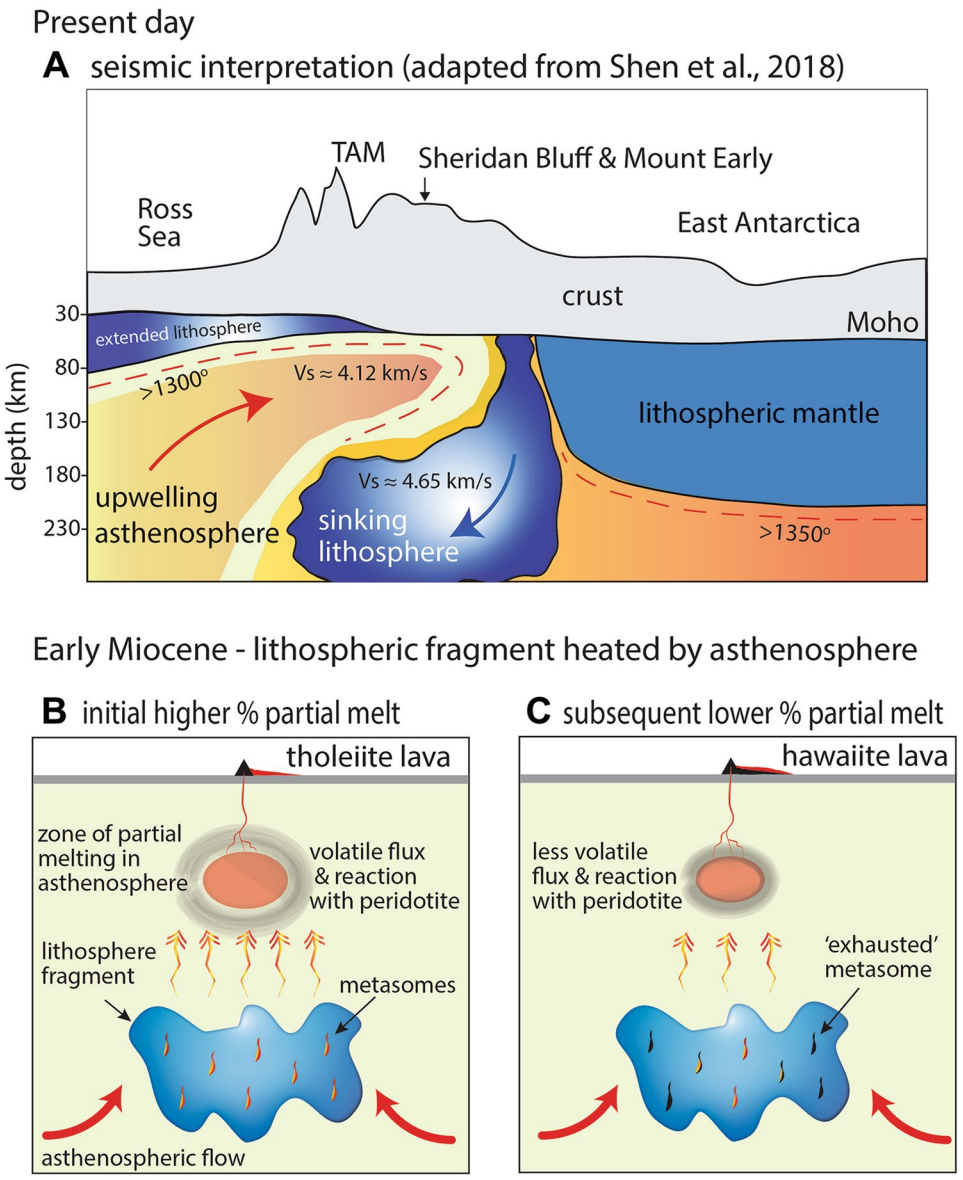

Fig. 12 (**A**) present day interpretation of the seismic shear wave velocity profile to 250 km depth across the southern Transantarctic Mountains adapted from Shen et al. (2018). At c. 80 km beneath Mount Early, Shen et al. (2018) recorded the slowest shear wave velocities ($V_S = 4.12$ km/sec) that are underlain at c. 200 km depth by relatively fast velocities ($V_s = 4.65$ km/sec). (**B**) Early Miocene (~ 20 Ma) detached fragments of metasomatized lithosphere reach temperatures to melt metasomes and release volatile-rich fluids into the overlying asthenosphere. At c. 100 km depth, wet melting of asthenosphere at relatively high degrees (5–6%) was concurrent with reaction between liquids and peridotite to produced silica-saturated tholeiitic melts. (**C**) successive melting at lower degrees (1.5–2%) and less reaction produced alkaline melts. The decrease in degree of partial melting was likely controlled by the exhaustion of volatile-rich phases (e.g., amphibole) in foundered lithospheric fragments

and is underlain at about 200 km depth by relatively fast seismic velocities that are interpreted to be foundered lithosphere (Shen et al. 2018). Density instability of mantle lithosphere can be caused by injections of mafic silicate melts and fluids beneath cratons. The metasomatic process is most likely related to melts and fluids generated during subduction of oceanic lithosphere along the paleo-Pacific margin of Gondwana in the late Paleozoic to the middle Mesozoic (described above). Shen et al. (2018) suggested that more than 100 million years after metasomatism the thick, cold, and heavy lithospheric lid became vulnerable to delamination when tectonic conditions were suitable. This may have been facilitated when extensional stresses migrated inboard from the developing West Antarctic rift system in the Late Cretaceous—Paleogene (Shen et al. 2018) or when motion between East and West Antarctica produced oblique convergence and flexural bending in the southern Transantarctic Mountains during the Neogene (Granot and Dyment 2018).

The process of detachment and sinking of lithosphere can produce melt by allowing asthenosphere to rise adiabatically. Decompressive melting of upwelling asthenosphere triggered by lithospheric detachments is used by Hoernle et al. (2006) to explain intraplate basaltic volcanism in New Zealand. Variability in the size and vertical extent of cavities left by these detachments is used to account for differences in degrees of partial melting to form the range of alkaline to subalkaline compositions that exist as well as differences in volcanic systems (i.e., monogenetic volcanic fields versus composite shield volcanoes). In addition or alternatively, portions (drips) of lithosphere can be warmed by conductive heating as they become engulfed by the convecting mantle (Kay and Kay

1993; Elkins-Tanton 2007; Ducea et al. 2013; Furman et al. 2016) and upon sinking and heating, metasomatized lithosphere will release volatiles into the surrounding mantle to promote flux melting (Elkins-Tanton 2007; Furman et al. 2016). Flux melting of asthenosphere triggered by lithospheric detachment applied to the Upper Scott Glacier Volcanic Field is used here to explain the field's enigmatic tectonic setting, its isolation from other occurrences of Cenozoic volcanism, and the melting conditions along with source compositions that produced the magmas erupted at Mount Early and Sheridan Bluff.

A model for volcanism

A model that describes the origin of the Upper Scott Glacier Volcanic Field must account for the change in degree of partial melting in generating both tholeiite and alkaline magma compositions and to explain their nearly simultaneous eruption from a small monogenetic center (i.e., Sheridan Bluff). It must also account for changes in Sr and Nd isotope compositions (Fig. 6A and B) while maintaining uniform oxygen (Fig. 5) and relatively uniform Pb (Fig. 6C and D) isotopic signatures. For this, we envisage a continuous melting process that was intimately linked with the delamination of subcontinental lithosphere as seismically imaged beneath this region by Shen et al. (2018).

To begin, heating of the detached metasomatized lithosphere produced melts and fluids that triggered wet melting of the asthenosphere (Fig. 12B). It is likely that these initial liquids were silica-undersaturated (i.e., melting of hydrous cumulates in the lithosphere composed mainly of amphibole and clinopyroxene) and thus would have reacted with orthopyroxene in peridotite to become more enriched in silica while crystallizing olivine (Shaw et al. 1998; Shaw 1999; Lundstrom et al. 2000). To evaluate this reaction, melting experiments using natural hornblendite (amphibole-rich veins) and a moderately depleted peridotite were performed at 1.5 GPa and 1200°−1325 °C by Pilet et al. (2008). The experiments demonstrate that this reaction will also evolve liquids with lower alkalinity, TiO_2, FeO (Figs. 2, 3A and B) and incompatible trace element contents (Figs. 7A and 9C). It will also produce slightly higher MgO and Al_2O_3 contents, while maintaining relatively constant Al_2O_3/TiO_2 ratios (Fig. 3C). The initial phase of higher degrees of partial melting and reaction with peridotite in the asthenosphere generated the tholeiite magmas. The depth of melting is estimated at between 90 and 120 km using the algorithms of Herzberg and Zhang (1996) and Wood (2004) for anhydrous melts. Our calculations using filtered data corrected for olivine fractionation (samples that achieved whole rock Mg# = 73 with the addition of less than 20% olivine) yield pressures that range from 2.8 to 3.5 GPa using Herzberg and Zhang (1996) empirically derived equations for Al_2O_3, FeO^T and MgO (wt.%). A much narrower but overlapping range from 2.7 to 2.9 GPa (c. 91 to 98 km) is calculated using the Wood (2004) barometer. Overall, the pressure estimates place the depth of flux melting at around 20 million years ago within the current lower seismic velocity zone and above the higher velocity zone that Shen et al. (2018) interpret as being detached lithosphere (Fig. 12A). With decreasing lithospheric flux, possibly caused by exhaustion of volatile-rich phases in the sinking fragments not long after temperatures exceeded their melting points (e.g., 1150−1175 °C for amphibole-rich cumulates: Pilet et al. 2008; Mandler and Grove 2016), the overall degree of partial melting within the asthenosphere also decreased (Fig. 12C). With lower degrees of melting and less orthopyroxene to react, subsequent liquids that were parental to hawaiite magmas retained a silica-undersaturated and trace element-enriched composition.

Summary and conclusions

Mafic compositions erupted at Mount Early and Sheridan Bluff volcanoes, Upper Scott Glacier Volcanic Field (USGVF), provide a rare glimpse of mantle geochemical domains and melting conditions beneath the eastern portion of the Antarctic continent but also offer insight on possible mechanisms and conditions for the generation of small volume, polymagmatic mafic systems found in West Antarctica and other intraplate continental settings worldwide. The Early Miocene volcanism consists of subalkaline and alkaline types classified as tholeiite, hawaiite and mugearite. Volcanic rocks from Mount Early and Sheridan Bluff are distinctive, both geochemically and isotopically, from the majority of volcanic rocks associated with the West Antarctic rift system but are akin to several monogenetic volcanic fields on its periphery and on the Antarctic Peninsula. Our study provides details indicating that:

- Neither fractional crystallization nor crustal assimilation can account for the relationship between coexisting tholeiite and alkaline lavas (i.e., hawaiite) at Sheridan Bluff. Their close association is explained by progressive changes in degrees of partial melting (i.e., from 5−6% for tholeiite down to 1.5−2% for alkaline magmas) and reaction between liquid and peridotite within a compositionally heterogeneous mantle.
- Mount Early and Sheridan Bluff compositions share many compositional characteristics with back-arc and post-subduction intraplate alkaline and tholeiite basalts from the Antarctic Peninsula and with basalts from two widely separated volcanic fields: one in western Marie Byrd Land (Fosdick Mountains) and the other in western Ellsworth Land (Jones Mountains). Altogether,

their relatively un-radiogenic Pb isotopic signatures and moderately enriched incompatible trace element concentrations suggest a mantle source that is similar to the mantle that sourced E-MORB compositions erupted along the Antarctic−Phoenix Ridge.

- A greater contribution from an enriched mantle source can explain the correlation between relatively radiogenic Sr isotope ratios (>0.7038 to ≤ 0.7048) and relatively un-radiogenic Nd isotope ratios (0.5127 to ≤ 0.5129). The Sr and Nd isotopic signatures and moderately elevated oxygen isotope values (average $\delta^{18}O = 5.5‰$) suggest the influence of an enriched mantle that was a source for Karoo−Ferrar magmatism in the Jurassic Period.
- The tapping of both depleted and enriched mantle sources was facilitated by the detachment, sinking and heating of metasomatized continental lithospheric mantle in the convecting mantle. We propose a scenario where initial melting in the asthenosphere occurred at a higher degree, triggered and aided by flux from the devolatilizing lithosphere (=enriched source). Higher amounts of melting and reaction of silica-undersaturated liquids with peridotite produced tholeiite magmas while diminishing melt production with less orthopyroxene available to react yielded alkaline magmas. Furthermore, we suggest that the progressive decrease in melt proportion was also accompanied by a decrease in the relative proportion of the enriched source to account for the change in Sr and Nd isotope ratios.
- Other small-volume, monogenetic, tholeiite–alkaline systems in West Antarctica and elsewhere may also be the expression of areas where localized lithospheric delamination allowed concurrent melting and mixing of compositionally distinct mantle sources for volcanism.

Finally, the timing of the detachment relative to the Early Miocene volcanism is poorly constrained. It has been estimated, based on the relative timing of extension and magmatism in the northern Ross Sea region, that it may have taken between 20 and 30 million years for metasomes at the base of subcontinental mantle lithosphere to reach their melting point via conductive heating by edge-driven mantle flow to produce the Cenozoic alkaline volcanism there (Panter et al. 2018). Beneath Mount Early and Sheridan Bluff in the southern Transantarctic Mountains, conductive heating would be facilitated by upwelling asthenosphere engulfing the sinking metasomatized lithosphere. Consequently, the initial detachment may have occurred significantly before the volcanism at around 40–50 million years ago. Interestingly, this time period coincides broadly with the initiation of the youngest exhumation event recorded in the Scott Glacier region (50−45 Ma; Fitzgerald and Stump 1997; Fitzgerald 2002) or the oldest event in the Shackleton Glacier region (40 Ma; Miller et al. 2010) that lies ~300 km to the north. Knowledge of the timing and cause of uplift is important in that it can provide constraints on heat flux from the mantle and contribute to our understanding of the rheology of the lithosphere to better constrain models for glacial isostatic adjustment.

Supplementary Information The online version contains supplementary material available at https://doi.org/10.1007/s00410-022-01914-9.

Acknowledgements We thank Ed Stump for providing local geological and logistical information prior to our 2015 expedition, Tim Burton for his invaluable assistance in the field and all U.S. Antarctic Program personnel in McMurdo and at the Shackleton Glacier transit camp for their logistical support. Gordon Moore and Owen Neill are thanked for their expertise and guidance in mineral analysis at the University of Michigan. John Valley assisted in analysis and interpretation of oxygen isotope ratios at the University of Wisconsin. Funding for this project was provided by a U.S. National Science Foundation grant NSF-PLR 1443576 (KSP) that helped to support thesis research for Y. Li and J. Reindel, and undergraduate research for K. Odegaard. MJS was supported by DOE grants (DE-FG02-93ER14389 and DE-SC0020666) to JV. We appreciate the comments provided by two anonymous reviewers along with the suggestions and the careful editorial handling of this manuscript by Othmar Müntener, altogether, significantly improving the presentation of our study.

References

Abouchami W, Galer SJG, Koschinsky A (1999) Pb and Nd isotopes in NE Atlantic Fe–Mn crusts: proxies for trace metal paleosources and paleocean circulation. Geochim Cosmochim Acta 63:1489–1505

Arth JG (1976) Behavior of trace elements during magmatic processes – a summary of theoretical models and their applications. J Res United States Geol Survey 4:41–47

Beattie P (1993) Olivine-melt and orthopyroxene-melt equilibria. Contrib Miner Petrol 115:103–111

Bohrson WA, Spera FJ, Heinonen JS, Brown GA, Scruggs MA, Adams JV, Takach MK, Zeff G, Suikkanen E (2020) Diagnosing open-system magmatic processes using the Magma Chamber Simulator (MCS): part I – major elements and phase equilibria. Contrib Miner Petrol 175:104. https://doi.org/10.1007/s00410-020-01722-z

Boyce, J. A., Nicholls, I. A., Keays, R. R. and Hayman, P. C. 2015. Variation in parental magmas of Mt. Rouse, a complex polymagmatic volcano in the basaltic intraplate Newer Volcanics Province, southeast Australia. Contributions to Mineralogy and Petrology 169: 11. https://doi.org/10.1007/s00410-015-1106-y.

Bredow, E., Steinberger, B., Gassmöller, R., Dannberg, J. 2021. Mantle convection and possible mantle plumes beneath Antarctica—insights from geodynamic models and implications for topography. In: Martin, A. P. and van der Wal, W. (Eds), *The Geochemistry and Geophysics of the Antarctic Mantle*. Geological Society, London, Memoir 56, https://doi.org/10.1144/M56-2020-2.

Brenna M, Cronin SJ, Smith IEM, Sohn YK, Németh K (2010) Mechanisms driving polymagmatic activity at a monogenetic volcano, Udo, Jeju Island, South Korea. Contrib Miner Petrol 160:931–950

Cande SC, Stock JM, Müller RD, Ishihara T (2000) Cenozoic motion between east and west Antarctica. Nature 404:145–150

Castillo P (2015) The recycling of marine carbonates and sources of HIMU and FOZO ocean island basalts. Lithos 216–217:254–263. https://doi.org/10.1016/j.lithos.2014.12.005

Cawood PA (2005) Terra Australis Orogen: Rodinia breakup and development of the Pacific and Iapetus margins of Gondwana during the Neoproterozoic and Paleozoic. Earth Sci Rev 69:249–279

Choe WH, Lee JI, Lee MJ, Hur SD, Jin YK (2007) Origin of E-MORB in a fossil spreading center: the Antarctic-Phoenix Ridge, Drake Passage. Antarctica Geosciences Journal 11(3):185–199

Choi S-H, Choe W-H, Lee J-I (2008) Mantle heterogeneity beneath the Antarctic-Phoenix Ridge off Antarctic Peninsula. Island Arc 17:172–182

Choi S-H, Mukasa SB, Ravizza G, Fleming TH, Marsh BD, Bédard JHJ (2019) Fossil subduction zone origin for magmas in the Ferrar Large Igneous Province, Antarctica: evidence from PGE and OS isotope systematics in the Basement Sill of the McMurdo Dry Valleys. Earth Planet Sci Lett 506:507–519. https://doi.org/10.1016/j.epsl.2018.11.027

Coltorti M, Beccaluva L, Bonadiman C, Faccini B, Ntaflos T, Siena F (2004) Amphibole genesis via metasomatic reaction with clinopyroxene in mantle xenoliths from Victoria Land, Antarctica. Lithos 75:115–139

Craddock C, Bastien TW, Rutford RH (1964) Geology of the Jones Mountains area. In: Adie RJ (ed) Antarctic Geology. North-Holland, Amsterdam, pp 171–187

D'Orazio M, Armienti P, Cerretini S (1998) Phenocryst/matrix trace-element partition coefficients for hawaiite-trachyte lavas from the Ellittico volcanic sequence (Mt. Etna, Sicily, Italy). Mineral Petrol 64:65–88

Dallai L, Ghezzo C, Sharp ZD (2003) Oxygen isotope evidence for crustal assimilation and magma mixing in the Granite Harbor Intrusives, Northern Victoria Land, Antarctica. Lithos 67:135–151

Demény A, Harangi Sz, Vennemann TW, Casillas R, Horváth P, Milton AJ, Mason PRD, Ulianov A (2012) Amphiboles as indicators of mantle source contamination: combined evaluation of stable H and O isotope compositions and trace element ratios. Lithos 152:141–156. https://doi.org/10.1016/j.lithos.2012.07.001

DiVenere VJ, Kent DV, Dalziel IWD (1994) Mid-Cretaceous paleomagnetic results from Marie Byrd Land, West Antarctica: A test of post-100 Ma relative motion between East and West Antarctica. J Geophys Res 99:15115

Doumani GA, Minshew VH (1965) General geology of the Mount Weaver area, Queen Maud Mountains. In: Hadley JB (ed) Geology and paleontology of the Antarctic. American Geophysical Union, Antarctic Research Series, 6, pp 127–139

Eiler JM, Farley KA, Valley JW, Hauri E, Craig H, Hart SR, Stolper EM (1997) Oxygen isotope variations in ocean island basalt phenocrysts. Geochimica Cosmochimica Acta 61(11):2281–2293

Eiler JM (2001) Oxygen isotope variations of basaltic lavas and upper mantle rocks. In: Valley JW, Cole D (eds) Stable Isotope Geochemistry. Mineralogical Society of America and Geochemical Society, Reviews in Mineralogy and Geochemistry, vol 43, pp 319–364

Elkins-Tanton LT (2007) Continental magmatism, volatile recycling, and a heterogeneous mantle caused by lithospheric gravitational instabilities. J Geophys Res 112:B03405. https://doi.org/10.1029/2005JB004072

Elliott, D. and Fleming, T. H. 2021. Ferrar Dolerite and Kirkpatrick Basalt Formations II. petrology. In: Smellie, J. L., Panter, K. S. and Geyer, A. (Eds.). *Volcanism in Antarctica: 200 Million Years of Subduction, Rifting and Continental Break-Up*. Geological Society, London, Memoirs 55, https://doi.org/10.1144/M55-2018-39.

Encarnación J, Grunow A (1996) Changing magmatic and tectonic styles along the paleo-Pacific margin of Gondwana and the onset of early Paleozoic magmatism in Antarctica. Tectonics 15(6):1325–1341. https://doi.org/10.1029/96TC01484

Ersoy EY, Helvacı C, Palmer MR (2010) Mantle source characteristics and melting models for the early-middle Miocene mafic volcanism in Western Anatolia: Implications for enrichment processes of mantle lithosphere and origin of K-rich volcanism in post-collisional settings. J Volcanol Geoth Res 198:112–128

Ferguson EM, Klein EM (1993) Fresh basalts from the Pacific-Antarctic Ridge extend the Pacific geochemical province. Nature 366(6453):330–333

Fitzgerald PG (2002) Tectonics and landscape evolution of the Antarctic plate since the breakup of Gondwana, with an emphasis on the West Antarctic Rift System and the Transantarctic Mountains. Antarctica at the close of a millennium. Royal Society of New Zealand Bulletin 35:453–469

Fitzgerald PG, Stump E (1997) Cretaceous and Cenozoic episodic denudation of the Transantarctic Mountains, Antarctica: new constraints from apatite fission track thermochronology in the Scott Glacier region. J Geophys Res 102:7747–7765

Floyd PA, Winchester JA (1975) Magma type and tectonic setting discrimination using immobile elements. Earth Planet Sci Lett 27(2):211–218. https://doi.org/10.1016/0012-821X(75)90031-X

Furman T, Nelson WR, Elkins-Tanton LT (2016) Evolution of the East African rift: drip magmatism, lithospheric thinning and mafic volcanism. Geochim Cosmochim Acta 185:418–434

Gaffney, A. M. and Siddoway, C. S. 2007. Heterogeneous sources for Pleistocene lavas of Marie Byrd Land, Antarctica: new data from the SW Pacific diffuse alkaline magmatic province. United States Geological Survey Open-File Report, 2007–1047, Extended Abstract 063.

Ghiorso MS, Sack RO (1995) Chemical Mass Transfer in Magmatic Processes IV. A revised and internally consistent thermodynamic model for the interpolation and extrapolation of liquid-solid equilibria in magmatic systems at elevated temperatures and pressures. Contrib Miner Petrol 119:197–212

Gómez-Ulla A, Sigmarsson O, Huertas MJ, Devidal J-L, Ancochea E (2018) The historical basanite—alkali basalt—tholeiite suite at Lanzarote, Canary Islands: carbonated melts of heterogeneous mantle source? Chem Geol 494:56–68. https://doi.org/10.1016/j.chemgeo.2018.07.015

Goodge JW (2020) Geological and tectonic evolution of the Transantarctic Mountains, from ancient craton to recent enigma. Gondwana Res 80:50–122. https://doi.org/10.1016/j.gr.2019.11.001

Granot R, Dyment J (2018) Late Cenozoic unification of East and West Antarctica. Nat Commun. https://doi.org/10.1038/s41467-018-05270-w

Haase KM, Beier C, Fretzdorff S, Leat PT, Livermore RA, Barry TL, Pearce JA, Hauff F (2011) Magmatic evolution of a dying spreading axis: evidence for the interaction of tectonics and mantle heterogeneity from the fossil Phoenix Ridge, Drake Passage. Chem Geol 280:115–125

Haase, K. M., Beier, C. 2021. Chapter 3.2b Bransfield Strait and James Ross Island: petrology. In: Smellie, J. L., Panter, K. S. and Geyer, A. (Eds.), *Volcanism in Antarctica: 200 Million Years of Subduction, Rifting and Continental Break-up*. Geological Society, London, Memoir 55, 285–301. https://doi.org/10.1144/M55-2018-37.

Hamelin C, Dosso L, Hanan BB, Moreira M, Kositsky AP, Thomas MY (2011) Geochemical portray of the Pacific Ridge: new isotopic data and statistical techniques. Earth Planet Sci Lett 302:154–162

Hart SR (1988) Heterogeneous mantle domains: signatures, genesis and mixing chronologies. Earth Planet Sci Lett 90:273–296

Hart SR, Hauri EH, Oschmann LA, Whitehead JA (1992) Mantle plumes and entrainment: Isotopic evidence. Science 256:517–520

Hart SR, Blusztajn J, Craddock C (1995) Cenozoic volcanism in Antarctica; Jones Mountains and Peter I Island. Geochim Cosmochim Acta 59:3379–3388

Heeszel DS, Wiens DA, Anandakrishnan S, Aster RC, Dalziel IWD, Huerta AD, Nyblade AA, Wilson TJ, Winberry JP (2016) Upper mantle structure of central and West Antarctica from array analysis of Rayleigh wave phase velocities. J Geophys Res Solid Earth 121:1758–1775

Heinonen JS, Carlson RW, Luttinen AV (2010) Isotopic (Sr, Nd, Pb, and Os) composition of highly magnesian dikes of Vestfjella, western Dronning Maud Land, Antarctica: a key to the origin of Jurassic Karoo large igneous province? Chem Geol 277:227–244

Heinonen JS, Luttinen AV, Whitehouse MJ (2018) Enrichment of ^{18}O in the mantle sources of the Antarctic portion of the Karoo large igneous province. Contrib Miner Petrol 173:21. https://doi.org/10.1007/s00410-018-1447-4

Heinonen JS, Bohrson WA, Spera FJ, Brown GA, Scruggs MA, Adams JV (2020) Diagnosing open-system magmatic processes using the Magma Chamber Simulator (MCS): part II—trace elements and isotopes. Contrib Miner Petrol 175:105. https://doi.org/10.1007/s00410-020-01718-9

Hergt JM, Peate DW, Hawkesworth CJ (1991) The petrogenesis of Mesozoic Gondwana low-Ti flood basalts. Earth Planet Sci Lett 105:134–148

Herzberg C, Zhang J (1996) Melting experiments on anhydrous peridotite KLB-1: compositions of magmas in the upper mantle and transition zone. J Geophys Res 101:8271–8295

Hoefs J, Faure G, Elliot DH (1980) Correlation of $\delta^{18}O$ and initial $^{87}Sr/^{86}Sr$ ratios in Kirkpatrick Basalt on Mt. Falla, Transantarctic Mountains. Contribution to Mineralogy and Petrology 75:199–203

Hoernle K, White JDL, van den Bogaard P, Hauff F, Coombs DS, Werner R, Timm C-S, Reay A, Cooper AF (2006) Cenozoic intraplate volcanism on New Zealand: upwelling induced by lithospheric removal. Earth Planet Sci Lett 248:350–367

Hofmann AW, Jochum KP, Seufert M, White WM (1986) Nb and Pb in oceanic basalts: new constraints on mantle evolution. Earth Planet Sci Lett 79:33–45

Hofmann, A.W. 2003. Nb-U-Th-La tracers of basalt sources revisited. American Geophysical Union, Fall Meeting 2003, abstract id.V52D-01. https://ui.adsabs.harvard.edu/#abs/2003AGUFM.V52D..01H/abstract.

Hofmann, A. W. 2007. 2.03-Sampling Mantle Heterogeneity through Oceanic Basalts: Isotopes and Trace Elements, In: Heinrich D. Holland and Karl K. Turekian, Editor(s)-in-Chief, Treatise on Geochemistry, Pergamon, Oxford, 2007, Pages 1–44, ISBN 9780080437514, https://doi.org/10.1016/B0-08-043751-6/02123-X.

Hole MJ (1988) Post-subduction alkaline volcanism along the Antarctic Peninsula. J Geol Soc London 145:985–998

Hole MJ (1990) Geochemical evolution of Pliocene-Recent post-subduction alkalic basalts from Seal Nunataks, Antarctic Peninsula. J Volcanol Geoth Res 40:149–167

Hole MJ, LeMasurier WE (1994) Tectonic controls on the geochemical composition of Cenozoic mafic alkaline volcanic rocks from West Antarctica. Contrib Miner Petrol 117:187–202

Hole MJ, Kempton PD, Millar IL (1993a) Trace-element and isotopic characteristics of small-degree melts of the asthenosphere: evidence from the alkalic basalts of the Antarctic Peninsula. Chem Geol 109:51–68

Hole MJ, Saunders AD, Rogers G, Sykes MA (1993b) The relationship between alkaline magmatism, lithospheric extension and slab window formation along continental destructive plate margins. Geol Soc Lond Spec Publ 81:265–285. https://doi.org/10.1144/GSL.SP.1994.081.01.15

Hole MJ, Storey BC, LeMasurier WE (1994) Tectonic setting and geochemistry of Miocene alkalic basalts from the Jones Mountains. West Antarctica Antarctic Science 6(1):85–92

Hole, M. J. 2021. Chapter 4.1b Antarctic Peninsula II. In: Smellie, J. L., Panter, K. S. and Geyer, A. (Eds.), *Volcanism in Antarctica: 200 Million Years of Subduction, Rifting and Continental Break-up*. Geological Society, London, Memoir 55, 327–343. https://doi.org/10.1144/M55-2018-40.

Huerta AD, Harry DL (2007) The transition from diffuse to focused extension: Modeled evolution of the West Antarctic Rift system. Earth Planet Sci Lett 255:133–147

Ionov DA, Hofmann AW (1995) Nb-Ta-rich mantle amphiboles and micas: Implications for subduction-related metasomatic trace element fractionations. Earth Planet Sci Lett 131:341–356

Ionov DA, Griffin WL, O'Reilly SY (1997) Volatile-bearing minerals and lithophile trace elements in the upper mantle. Chem Geol 141:153–184

Irvine TN, Baragar WRA (1971) A guide to the chemical classification of the common volcanic rocks. Can J Earth Sci 8(5):523–548

Ivanov AV, Meffre S, Thompson J, Corfu F, Kamenetsky VS, Kamenetsky MB, Demonterova EI (2017) Timing and genesis of the Karoo-Ferrar large igneous province: New high precision U-Pb data for Tasmania confirm short duration of the major magmatic pulse. Chem Geol 455:32–43

Jackson MG, Hart SR, Koppers AAP, Staudigel H, Konter J, Blusztajn J, Kurz M, Russell JA (2007) The return of subducted continental crust in Samoan lavas. Nature 448:684–687. https://doi.org/10.1038/nature06048

Johnson GL, Kyle PR, Vanney JR, Campsie J (1982) Geology of Scott and Balleny Islands, Ross Sea, Antarctica, and morphology of adjacent seafloor. NZ J Geol Geophys 25(4):427–436

Jung S, Masberg P (1998) Major- and trace-element systematics and isotope geochemistry of Cenozoic mafic volcanic rocks from the Vogelsberg (central Germany). Constraints on the origin of continental alkaline and tholeiitic basalts and their mantle sources. J Volcanol Geoth Res 86:151–177

Kay RW, Kay SM (1993) Delamination and delamination magmatism. Tectonophysics 219(1–3):177–189

Kipf A, Hauff F, Werner R, Gohl K, van den Bogaard P, Hoernle K, Maicher D, Klügel A (2014) Seamounts off the West Antarctic margin: A case for non-hotspot driven intraplate volcanism. Gondwana Res 25:1660–1679

Kocaarlson A, Yalçın Ersoy E (2018) Petrologic evolution of Miocene-Pliocene mafic volcanism in the Kangal and Gürün basins (Sivas-Malatya), central east Anatolia: Evidence for Miocene anorogenic magmas contaminated by continental crust. Lithos 310–311:392–408

Košler J, Magna T, Mlcoch B, Mixa P, Nyvlt D, Holub FV (2009) Combined Sr, Nd, Pb and Li isotope geochemistry of alkaline lavas from northern James Ross Island (Antarctic Peninsula) and implications for back-arc magma formation. Chem Geol 258:207–218

Krans, S. R. 2013, New mineral chemistry and oxygen isotopes from alkaline basalts in the northwest Ross Sea, Antarctica: insights on magma genesis across rifted continental and oceanic lithosphere. M.Sc. thesis, Bowling Green State University, 101 pp.

Kress VC, Carmichael ISE (1991) The compressibility of silicate liquids containing Fe2O3 and the effect of composition, temperature, oxygen fugacity and pressure on their redox states. Contrib Miner Petrol 108:82–92. https://doi.org/10.1007/BF00307328

Kyle PR (1990) A. McMurdo Volcanic Group Western Ross embayment. In: LeMasurier WE, Thomson JW (eds) Volcanoes of the Antarctic plate and southern Oceans, Antarctic Research Series 48. American Geophysical Union, Washington, pp 18–145

Kyle, P. R., Pankhurst, R. J., Bowman, J. R. 1983. Isotopic and chemical variation in Kirkpatrick Basalt Group rocks from southern Victoria Land. In: Oliver, R.L.; Jame, P.R.; Jago, J.B., (eds.) Antarctic earth science. Proceedings of the Fourth International Symposium on Antarctic Earth Sciences. Adelaide, August 1982. Canberra, Cambridge, Australian Academy of Science, Cambridge University Press, 234–237.

Larter RD, Barker PF (1991) Effects of ridge crest trench interaction on Antarctic Phoenix spreading forces on a young subducting plate. J Geophys Res 96:19583–19607

Le Bas MJ, Le Maitre RW, Streckeisen A, Zanettin B (1986) Chemical classification of volcanic rocks based on the total alkali-silica diagram. J Petrol 27:745–750

LeMasurier WE, Rex DC (1989) Evolution of linear volcanic ranges in Marie Byrd Land, West Antarctica. J Geophys Res 94:7223–7236

LeMasurier WE, Thomson JW (1990) *Volcanoes of the Antarctic plate and southern Oceans*. Antarctic Research Series 48. American Geophysical Union, Washington, p 487

Li Y (2020) Petrologic insights into basaltic magma genesis beneath East Antarctica. Thesis, Bowling Green State University, M.Sc, p 106

Licht KJ, Groth T, Townsend JP, Hennessy AJ, Hemming SR, Flood TP, Studinger M (2018) Evidence for extending anomalous Miocene volcanism at the edge of the East Antarctic craton. Geophys Res Lett 45:3009–3016

Livermore R, Balanya JC, Maldonado A, Martinez JM, Rodriguez-Fernandez J, Galdeano CS, Zaldivar JG, Jabaloy A, Barnolas A, Somoza L, Hernandez-Molina J, Surinach E, Viseras C (2000) Autopsy on a dead spreading center: The Phoenix Ridge, Drake Passage, Antarctica. Geology 28:607–610

Lundstrom CC, Gill J, Williams Q (2000) A geochemically consistent hypothesis for MORB generation. Chem Geol 162:105–126

Lustrino M, Melluso L, Morra V (2002) The transition from alkaline to tholeiitic magmas: a case study from the Orosei-Dorgali Pliocene volcanic district (NE Sardinia, Italy). Lithos 63(1–2):83–113. https://doi.org/10.1016/S0024-4937(02)00113-5

Luttinen AV (2018) Bilateral geochemical asymmetry in the Karoo large igneous province. Sci Rep 8:5223. https://doi.org/10.1038/s41598-018-23661-3

Luttinen AV, Furnes H (2000) Flood basalts of Vestfjella: Jurassic magmatism across an Archean-Proterozoic lithospheric boundary in Dronning Maud Land, Antarctica. J Petrol 41:1271–1305

Luttinen AV, Vuori SK (2006) Geochemical correlations between Jurassic gabbros and basaltic rocks in Vestfjella, Droning Maud Land, Antarctica. In: Hanski E, Mertanen S, Ramo T, Vuollo J (eds) Dyke swarms – time markers of crustal evolution. Taylor & Francis Group, London, pp 201–212

Luyendyk BP (1995) Hypothesis for Cretaceous rifting of east Gondwana caused by subducted slab capture. Geology 23:373–376

Luyendyke B, Cisowski S, Smith C, Richard S, Kimbrough D (1996) Paleomagnetic study of the northern Ford Ranges, western Marie Byrd Land, West Antarctica: mortion between West and East Antarctica. Tectonics 15:122–141

Mandler BE, Grove TL (2016) Controls on the stability and composition of amphibole in the Earth's mantle. Contrib Miner Petrol 171:68. https://doi.org/10.1007/s00410-016-1281-5

Martin A. P., Cooper, A., Price, R., Kyle, P., Gamble, J. 2021. Chapter 5.2b Erebus Volcanic Province II. Petrology. In: Smellie, J. L., Panter, K. S. and Geyer, A. (Eds.), *Volcanism in Antarctica: 200 Million Years of Subduction, Rifting and Continental Break-up*. Geological Society, London, Memoir 55, 447–489. https://doi.org/10.1144/M55-2020-10.

Mattey D, Lowry D, Macpherson C (1994) Oxygen isotope composition of mantle peridotite. Earth Planet Sci Lett 128:231–241

McDonough WF, Sun SS (1995) The Composition of the Earth. Chem Geol 120(3–4):223–253

McGee LE, Millet M-A, Smith IEM, Németh K, Lindsay JM (2012) The inception and progression of melting in a monogenetic eruption: Motukorea Volcano, the Auckland Volcanic Field, New Zealand. Lithos 155:360–374

Mensing TM, Faure G, Jones LM, Bowman JR, Hoefs J (1984) Petrogenesis of the Kirkpatrick Basalt, Solo Nunatak, northern Victoria Land, Antarctica, based on isotopic compositions of strontium, oxygen and sulfur. Contrib Miner Petrol 87:101–108

Miller, S.R., Fitzgerald, P.G., Baldwin, S.L. 2010. Cenozoic range-front faulting and development of the Transantarctic Mountains near Cape Surprise, Antarctica: thermochronologic and geomorphologic constraints. Tectonics 29, doi:https://doi.org/10.1029/2009TC002457

Moine BN, Grégorie M, O'Reilly SY, Sheppard SMF, Cottin JY (2001) High field strength element fractionation in the upper mantle: evidence from amphibole-rich composite mantle xenoliths from the Kerguelen Islands (Indian Ocean). J Petrol 42(11):2145–2167. https://doi.org/10.1093/petrology/42.11.2145

Molnar P, Atwater T, Mammerickx J, Smith SM (1975) Magnetic anomalies, bathymetry and the tectonic evolution of the South Pacific since the Late Cretaceous. Geophys J Int 40:383–420

Molzahn M, Reisberg L, Worner G (1996) Os, Sr, Nd, Pb, O isotope and trace element data from the Ferrar flood basalts, Antarctica: evidence for an enriched subcontinental lithospheric source. Earth Planet Sci Lett 144:529–546

Moore JG, Hickson CJ, Calk LC (1995) Tholeiitic-alkalic transition at subglacial volcanoes, Tuya region, British Columbia. Canada Journal of Geophysical Research-Solid Earth 100(B12):24577–24592. https://doi.org/10.1029/95JB02509

Mortimer, N., Dunlap, W. J., Isaac, M. J., Sutherland, R. P., Faure, K. 2007. Basal Adare volcanics. Robertson Bay, North Victoria Land, Antarctica: Late Miocene intraplate basalts of subaqueous origin, In A.K. Cooper & C.R. Raymond et al. (Eds), Proceedings of the 10th International Symposium on Antarctic Earth Sciences, USGS Open-File Report 2007–1047, Short Research Paper 045, 7 p., doi: https://doi.org/10.3133/ofr20071047srp045.

Nakamura E, Campbell IH, Sun S-S (1985) The influence of subduction processes on the geochemistry of Japanese alkaline basalts. Nature 316:55–58

Nardini I, Armienti P, Rocchi S, Dallai L, Harrison D (2009) Sr-Nd-Pb-He-O Isotope and Geochemical Constraints on the Genesis of Cenozoic Magmas from the West Antarctic Rift. J Petrol 50:1359–1375

Needham AJ, Lindsay JM, Smith IEM, Augustinus P, Shane PA (2011) Sequential eruption of alkaline and sub-alkaline magmas from a small monogenetic volcano in the Auckland Volcanic Field, New Zealand. J Volcanol Geoth Res 201:126–142

Nelson DA, Cottle JM (2017) Long-term geochemical and geodynamic segmentation of the paleo-Pacific margin of Gondwana: insight from the Antarctic and adjacent Sectors. Tectonics 36:3229–3247

Panter KS, Castillo P, Krans S, Deering C, McIntosh W, Valley JW, Kitajima K, Kyle P, Hart S, Blusztajn J (2018) Melt origin across a rifted continental margin: a case for subduction-related metasomatic agents in the lithospheric source of alkaline basalt, northwest Ross Sea. Antarctica Journal of Petrology 59(3):517–558. https://doi.org/10.1093/petrology/egy036

Panter KS, Martin AP (2021) West Antarctic mantle deduced from mafic magmatism. In: Martin AP, van der Wal W (eds) The Geochemistry and Geophysics of the Antarctic Mantle. Geological Society, London, Memoir 56, https://doi.org/10.1144/M56-2021-10

Panter KS, Reindel J, Smellie JL (2021a) Chapter 5.3b Mt. Early & Sheridan Bluff II. Petrology. In: Smellie JL, Panter KS, Geyer A (eds) Volcanism in Antarctica: 200 Million Years of Subduction,

Rifting and Continental Break-up. Geological Society, London, Memoir 55, p 499–514. https://doi.org/10.1144/M55-2020-10.
Panter KS, Wilch TI, Smellie JL, Kyle PR, McIntosh WC (2021b) Chapter 5.4b Marie Byrd Land & Ellsworth Land II: petrology. In: Smellie JL, Panter KS, Geyer A (eds), Volcanism in Antarctica: 200 Million Years of Subduction, Rifting and Continental Break-up. Geological Society, London, Memoir 55, p 577–614. https://doi.org/10.1144/M55-2019-50.
Panter KS (2021) petrology and tectonomagmatic overview, Chapter 1.3. In: Smellie JL, Panter KS, Geyer A (eds.) Volcanism in Antarctica: 200 Million Years of Subduction, Rifting and Continental Break-Up. Geological Society, London, Memoir 55, p 43–53. https://doi.org/10.1144/M55-2020-10.
Perinelli C, Armienti P, Dallai L (2006) Geochemical and O-isotope constraints on the evolution of lithospheric mantle in the Ross Sea rift area (Antarctica). Contrib Miner Petrol 151:245–266
Perinelli C, Gaeta M, Armienti P (2017) Cumulate xenoliths from Mt. Overlord, northern Victoria Land, Antarctica: a window into high pressure storage and differentiation of mantle-derived basalts. Lithos 268–271:225–239
Pilet S, Baker MB, Stolper EM (2008) Metasomatized lithosphere and the origin of alkaline lavas. Science 320:916–919
Pilet S, Baker MB, Muntener O, Stolper EM (2011) Monte Carlo Simulations of Metasomatic Enrichment in the Lithosphere and Implications for the Source of Alkaline Basalts. J Petrol 52:1415–1442
Prestvik T, Barnes CG, Sundvoll B, Duncan RA (1990) Petrology of Peter I Øy (Peter I Island), West Antarctica. J Volcanol Geoth Res 44:315–338. https://doi.org/10.1016/0377-0273(90)90025-B
Putirka K, Perfit M, Ryerson FJ, Jackson MG (2007) Ambient and excess mantle temperatures, olivine thermometry, and active vs. passive upwelling. Chem Geol 241:177–206
Putirka, K. 2008. Thermometers and Barometers for Volcanic Systems. In Putirka, K., Tepley, F. (Eds.), Minerals, Inclusions and Volcanic Processes, Reviews in Mineralogy and Geochemistry, Mineralogical Soc. Am., 69, 61–120.
Rapela, C. W., Pankhurst, R. J., Fanning, C. M., Herve, F. 2005. Pacific subduction coeval with the Karoo mantle plume: the early Jurassic subcordilleran belt of northwestern Patagonia. In: Vaughan, A.P.M.; Leat, P.T.; Pankhurst, R.J., (eds.) Terrane processes at the margins of Gondwana. Geological Society of London Special Publication 246, 217–239.
Reindel JL (2018) The origin of basalt and cause of melting beneath East Antarctica as revealed by the southernmost volcanoes on Earth. Thesis, Bowling Green State University, M.Sc, p 92
Rocchi S. and Smellie J. L. 2021. Chapter 5.1b Northern Victoria Land II. petrology. In: Smellie, J. L., Panter, K. S. and Geyer, A. (Eds.), *Volcanism in Antarctica: 200 Million Years of Subduction, Rifting and Continental Break-up*. Geological Society, London, Memoir 55, 383–413. https://doi.org/10.1144/M55-2019-19.
Rodgers NW, Hawkesworth CJ, Mattey DP (1987) Sediment subduction and the source of potassium in orogenic leucitites. Geology 15:451–453
Roeder PL, Emslie RF (1970) Olivine-liquid equilibrium. Contrib Miner Petrol 29:275–289
Rudnick, R. L. and Gao, S. 2003. Composition of the Continental Crust. In: R. L. Rudnick, H. D. Holland and K. K. Turekian (Eds.), Treatise on Geochemistry, Volume 3, 1–64.
Rutford, R. H., McIntosh, W. C. 2007. Jones Mountains, Antarctica: evidence for Tertiary glaciation revisited. In: Cooper, A. K., Barrett, P. J., Stagg, H., Storey, B., Stump, E. (Eds.), Antarctica: A Keystone in a Changing World−Online Proceedings of the 10th ISAES. U. S. Geological Survey Open-File Report 2007–1047, Extended Abstract 203, 5 p.
Saal AE, Kurz MD, Hart SR, Blusztajn JS, Blichert-Toft J, Liang Y, Geist DJ (2007) The role of lithospheric gabbros on the composition of Galapagos lavas. Earth Planet Sci Lett 257(3–4):391–406. https://doi.org/10.1016/j.epsl.2007.02.040
Shaw DM (1970) Trace element fractionation during anatexis. Geochim Cosmochim Acta 34:237–243
Shaw CS (1999) Dissolution of orthopyroxene in basanitic magma between 0.4 and 2 GPa: further implications for the origin of Si-rich alkaline glass inclusions in mantle xenoliths. Contrib Miner Petrol 135:114–132
Shaw CS, Thibault Y, Edgar AD, Lloyd FE (1998) Mechanisms of orthopyroxene dissolution in silica-undersaturated melts at 1 atmosphere and implications for the origin of silica-rich glass in mantle xenoliths. Contrib Miner Petrol 132:354–370
Shen W, Wiens DA, Stern T, Anandakrishnan S, Aster RA, Dalziel I, Hansen S, Heeszel DS, Huerta A, Nyblade A, Wilson TJ, Winberry JP (2018) Seismic evidence for lithospheric foundering beneath the southern Transantarctic Mountains, Antarctica. Geology 46:71–74
Sims KWW, DePaolo DJ (1997) Inferences about mantle magma sources from incompatible element concentration ratios in oceanic basalts. Geochim Cosmochim Acta 61(4):765–784. https://doi.org/10.1016/S0016-7037(96)00372-9
Sisson TW, Grove TL (1993) Temperatures and H2O contents of low-MgO high-alumina basalts. Contrib Miner Petrol 113:167–184
Smellie JL (1987) Geochemistry and tectonic setting of alkaline volcanic rocks in the Antarctic Peninsula: a review. J Volcanol Geoth Res 32:269–285
Smellie JL, Panter KS (2021) Lithofacies and eruptive conditions of the southernmost volcanoes in the world (87°S). Bull Volcanol 83:49. https://doi.org/10.1007/s00445-021-01475-y
Smellie JL, Panter KS, Geyer A (eds) (2021a) Volcanism in Antarctica: 200 Million Years of Subduction, Rifting and Continental Break-Up. Geological Society, London, Memoir 55, p 816. https://doi.org/10.1144/M55-2020-14.
Smellie JL, Panter KS, Reindel J (2021b) Chapter 5.3a Mt Early & Sheridan Bluff I. volcanology. In: Smellie JL, Panter KS, Geyer A (eds) Volcanism in Antarctica: 200 Million Years of Subduction, Rifting and Continental Break-up. Geological Society, London, Memoir 55, p 491–498. https://doi.org/10.1144/M55-2020-10.
Smith IEM, Németh K (2017) Source to surface model of monogenetic volcanism: a critical review. In: Németh K, Carrasco-Núñez G, Aranda-Gómez JJ, Smith IEM (eds) Monogenetic Volcanism. Geological Society, London, Special Publications, 446, p 1–28. https://doi.org/10.1144/SP446.14.
Stracke A, Hofmann AW, Hart SR (2005) FOZO, HIMU, and the rest of the mantle zoo: Geochemistry, Geophysics. Geosystems 6:Q05007. https://doi.org/10.1029/2004GC000824
Stump E, Sheridan MF, Borg SG, Sutter JF (1980) Early Miocene subglacial basalts, East Antarctic Ice Sheet, and uplift of the Transantarctic Mountains. Science 207:757–759
Stump, E., Borg, S. G. and Sheridan, M. F. 1990a. Sheridan Bluff. In: LeMasurier, W.E. and Thomson, J.W. (eds) Volcanoes of the Antarctic plate and southern oceans. American Geophysical Union, Antarctic Research Series, 48, pp. 136–137.
Stump, E., Borg, S. G. and Sheridan, M. F. 1990b. Mount Early. In: LeMasurier, W.E. and Thomson, J.W. (eds) Volcanoes of the Antarctic plate and southern oceans. American Geophysical Union, Antarctic Research Series, 48, pp. 138–139.
Sushchevskaya NM, Belyatsky BV, Leichenkov GL, Laiba AA (2009) Evolution of the Karoo-Maud mantle plume in Antarctica and its influence on the magmatism of the early stages of Indian Ocean opening. Geochem Int 47(1):1–17
Tiepolo M, Vannucci R, Oberti R, Foley S, Bottazzi P, Zanetti A (2000b) Nb and Ta incorporation and fractionation in titanian pargasite and kaersutite: crystal-chemical constraints and implications for natural systems. Earth Planet Sci Lett 176:185–201

Tiepolo, M., Vannucci, R., Bottazzi, P., Oberti, R., Zanetti, A., Foley, S. 2000a. Partitioning of rare earth elements, Y, Th, U, and Pb between pargasite, kaersutite, and basanite to trachyte melts: Implications for percolated and veined mantle. Geochemistry, Geophysics, Geosystems 1, paper number 2000aGC000064.

Tiepolo, M., Oberti, R., Zanetti, A., Vannucci, R., Foley, S. F. 2007. Trace-Element Partitioning Between Amphibole and Silicate Melt. In: Hawthorne, F. C., Oberti, R., Della Ventura, G. & Mottana, A. (eds) Amphiboles: Crystal Chemistry, Occurrence and Health Issues. Mineralogical Society of America and Geochemical Society, Reviews in Mineralogy and Geochemistry 67, 417–452.

Todt, W., Cliff, R.A., Hanser, A., Hofmann, A.W. 1996. Evaluation of a 202Pb-205Pb double spike for high-precision lead isotope analysis, in Earth Processes: Reading the Isotopic Code. Geophysical Monographs, Series 95, edited by A. Basu, and S. R. Hart, pp. 429–437, AGU, Washington, D.C.

Valley, J. W., Kitchen, N., Kohn, M. J., Niendorf, C. R., Spicuzza, M. J. 1995. UWG-2, a garnet standard for oxygen isotope ratios: Strategies for high precision and accuracy with laser heating: Geochimica et Cosmochimica Acta 59, 5223–5231.

Van Otterloo J, Raveggi M, Cas RAF, Maas R (2014) Polymagmatic activity at the monogenetic Mt Gambier Volcanic Complex in the Newer Volcanics Province, SE Australia: new insights into the occurrence of intraplate volcanic activity in Australia. J Petrol 55:1317–1351

Vlastélic I, Aslanian D, Dosso L, Bougault H, Olivet JL, Géli L (1999) Large-scale chemical and thermal division of the Pacific mantle. Nature 399:345–350

Wanless V, Garcia M, Rhodes J, Weis D, Norman MD (2006) Shield-stage alkalic volcanism on Mauna Loa Volcano, Hawaii. J Volcanol Geoth Res 151:141–155

Wilch, T. I., McIntosh, W. C., Panter, K. S. 2021. Chapter 5.4a Marie Byrd Land & Ellsworth Land I. Volcanology. In: J.L. Smellie, K.S. Panter, A. Geyer (Eds.), *Volcanism in Antarctica: 200 Million Years of Subduction, Rifting and Continental Break-Up*. Geological Society, London, Memoir 55, 515–576. https://doi.org/10.1144/M55-2019-39.

Wood BJ (2004) Melting of fertile peridotite with variable amounts of H2O. Washington DC American Geophysical Union Geophysical Monograph Series 150:69–80

Workman RK, Hart SR, Jackson MG, Regelous M, Farley KA, Blusztajn J, Kurz J, Staudigel H (2004) Recycled metasomatized lithosphere as the origin of the Enriched Mantle II (EM2) end-member: evidence from the Samoan Volcanic Chain Geochemistry, Geophysics. Geosystems 5:Q04008

Workman RK, Eiler JM, Hart SR, Jackson MG (2008) Oxygen isotopes in Samoan lavas: Confirmation of continent recycling. Geology 36(7):551–554

Zhao, Z-H., Zhang, G-L., Wang, S., Zhao, J-X. 2022. Origin of arc-like intraplate volcanism by melting of lithospheric mantle pyroxenite of the South China continental margin. Lithos 396-397. https://doi.org/10.1016/j.lithos.2021.106236

Zhao Z-F, Zheng Y-F (2003) Calculation of oxygen isotope fractionation in magmatic rocks. Chem Geol 193:59–80